REPORT DOCUMENTATION PAGE

Form Approved
OMB No. 0704-0188

1. AGENCY USE ONLY (Leave blank)	2. REPORT DATE	3. REPORT TYPE AND DATES COVERED
	1/3/96	Final Report 3/31/90 to 12/31/94

4. TITLE AND SUBTITLE

The Structure of Laminar Flames of CH_4/NO_2, CH_2O/NO_2, & HCN/NO_2

5. FUNDING NUMBERS

DAAL03-90-G-0084

6. AUTHOR(S)

Dr. Kalyanasundaram Seshadri

7. PERFORMING ORGANIZATION NAME(S) AND ADDRESS(ES)

Center for Energy and Combustion Research
Department of Applied Mechanics and Engineering Sciences
The University of California at San Diego
La Jolla, California 92093-0411

8. PERFORMING ORGANIZATION REPORT NUMBER

9. SPONSORING / MONITORING AGENCY NAME(S) AND ADDRESS(ES)

U.S. Army Research Office
P.O. Box 12211
Research Triangle Park, NC 27709-2211

10. SPONSORING / MONITORING AGENCY REPORT NUMBER

ARO 27455.11-EG

11. SUPPLEMENTARY NOTES

The views, opinions and/or findings contained in this report are those of the author(s) and should not be construed as an official Department of the Army position, policy, or decision, unless so designated by other documentation.

12a. DISTRIBUTION / AVAILABILITY STATEMENT

Approved for public release; distribution unlimited.

12b. DISTRIBUTION CODE

-

13. ABSTRACT *(Maximum 200 words)*

The principal objective of this research is to develop chemical-kinetic models which can be employed to model the combustion of solid propellants. The research was performed in collaboration with scientists at the U. S. Army Research Laboratory at Aberdeen Proving Grounds, Maryland. The gas phase combustion over the burning surface of many solid propellants take place in three zones—the primary reaction zone, the dark zone and the secondary reaction zone. This study was focused on characterizing the structures of the secondary reaction zone and the dark zone. The research comprised several studies. They were 1) studies on the structures of CH_4/NO_2 and CH_2O/NO_2 flames which are considered to be subsystems of the gas phase combustion taking place in the secondary reaction zone, 2) studies on the structures of hydrocarbon-air and alcohol-air flames which are useful for modeling CH_4/NO_2 and CH_2O/NO_2 flames, 3) studies on the structure of the dark zone formed over the burning surface of many solid propellants. Simplified and reduced chemical-kinetic mechanisms are deduced to describe chemical reactions taking place in these systems.

14. SUBJECT TERMS	15. NUMBER OF PAGES
combustion, propulsion, flame structure.	58
	16. PRICE CODE

17. SECURITY CLASSIFICATION OF REPORT	18. SECURITY CLASSIFICATION OF THIS PAGE	19. SECURITY CLASSIFICATION OF ABSTRACT	20. LIMITATION OF ABSTRACT
UNCLASSIFIED	UNCLASSIFIED	UNCLASSIFIED	UL

NSN 7540-01-280-5500

Standard Form 298 (Rev 2-89)
Prescribed by ANSI Std Z39-18
298-102

THE STRUCTURE OF LAMINAR FLAMES OF CH_4/NO_2, CH_2O/NO_2 AND HCN/NO_2

FINAL REPORT

K. SESHADRI

JANUARY 3, 1996

U. S. ARMY RESEARCH OFFICE

CONTRACT/GRANT NUMBER
DAAL03-90-G-0084

CENTER FOR ENERGY AND COMBUSTION RESEARCH
DEPARTMENT OF APPLIED MECHANICS AND ENGINEERING SCIENCES
UNIVERSITY OF CALIFORNIA AT SAN DIEGO
LA JOLLA, CALIFORNIA 92093-0411

Contents

Chapter 1

Introduction

1.1 Statement of the Problem

The research conducted here is relevant to combustion of solid propellants. The principal objective of this research is to develop chemical-kinetic models which can be employed to model the combustion of solid propellants. The research was performed in collaboration with scientists at the U. S. Army Research Laboratory at Aberdeen Proving Grounds, Maryland.

The physical and chemical processes that govern the ignition and combustion of solid propellants are complex. Several zones have been identified during combustion of propellants (Kubota 1981). Within the propellant, phase decomposition reactions take place. At the surface of the regressing propellant the solid melts and then vaporizes and significant exothermic reactions take place in the liquid phase. In the liquid layer on the surface of the propellant bubbles develop producing a "foam" reaction zone. Above the "foam" zone many propellants exhibit a two-stage flame zone. In this two-stage zone a nonluminous region separates the primary reaction zone near the surface of the propellant from the luminous secondary flame zone. The nonluminous region is commonly referred to as the dark zone. In the primary reaction zone the decomposition of the solid propellant takes place and moderately reactive intermediate species are formed. These intermediate species are convected away from the surface and they ignite after a short period of time. Combustion then continues in the secondary reaction zone. Previous studies have demonstrated the importance of the secondary reaction zone in controlling the burning rate of neat RDX (Melius 1986, Melius 1987, Melius 1988, Melius 1989). Recent experiments show that chemical effects caused by the use of propellants of different chemical composition can lead to major differences in ignition delays times during typical large calibre gun ballistics cycles (Kooker, Chang & Howard 1993, Kooker, Chang & Howard 1994, Kooker, Chang & Howard 1995, Kooker 1995). It is believed that the differences in ignition delay times for different propellants arise from differences in the chemistry

taking place in the dark zone (Kooker et al. 1995, Kooker 1995). The focus of this study is to investigate the structure of the secondary reaction zone and the structure of the dark zone.

The gas-phase combustion of propellants takes place in a number of subsystems, and the reactions between CH_4-NO_2 and CH_2O-NO_2 are such subsystems. An improved understanding of the chemistry taking place in these systems can be useful in modeling the combustion of solid propellants. A clear understanding of the structure of hydrocarbon air and alcohol air flames is required to model the structure of CH_4-NO_2 and CH_2O-NO_2 chemical systems. The research comprised several studies. They were 1) studies on the structures of CH_4-NO_2 and CH_2O-NO_2 flames, 2) studies on the structures of hydrocarbon-air and alcohol-air flames, and 3) studies on the structure of the dark zone formed over the burning surface of solid propellants. The results of these studies are summarized in the following publications and Ph.D theses.

1.2 Publications and Ph.D Theses

1.2.1 Publications

The papers published and those submitted for publication using support from this research program are

1. Bui, M., Seshadri, K., Williams, F. A., "The Asymptotic Structure of Premixed Methane-Air Flames with Slow CO Oxidation," *Combust. Flame* **89** (1992), pp 343–362.

2. Chelliah, H., Bui-Pham, M., Seshadri, K., and Law, C. K., "Numerical Description of the Structure of Counterflow Heptane-Air Flames Using Detailed and Reduced Chemistry with Comparisons to Experiments," *Twenty-Fourth Symposium (International) on Combustion,* The Combustion Institute, 1992, pp 851–857.

3. Yang, B., and Seshadri, K., "Asymptotic Analysis of the Structure of Nonpremixed Methane Air Flames using Reduced Chemistry," *Combust. Sci. and Tech.* **88** (1992), pp 115–132.

4. Yang, B., Seshadri, K., and Peters, N., "The Asymptotic Structure of Premixed Methanol-Air Flames," *Combust. Flame* **91** (1992), pp 382–398.

5. Chelliah, H. K., Seshadri, K., and Law, C. K., "Reduced Kinetic Mechanisms for Counterflow Methane-Air Diffusion Flames," in Reduced Kinetic Mechanisms for Applications in Combustion Systems (Eds. N. Peters and B. Rogg), *Lecture Notes in Physics,* **m 15**, Springer-Verlag, Heidelberg, 1993, pp 224–240.

6. Seshadri, K., and Williams, F. A., "Reduced Chemical Systems and their Applications in Turbulent Combustion," Chapter four in *Turbulent Reactive Flows (Eds. P. A. Libby and F. A. Williams)*, Academic Press, New York, 1994, pp 153–210.

7. Yang, B. and Seshadri, K., "The Asymptotic Structure of Methanol-Air Diffusion Flames," *Combust. Sci. and Tech.* **97** (1994), pp 193–218.

8. Trees, D., Brown, T. M., Seshadri, K., Smooke, M. D., Balakrishnan, G., Pitz, R. W., Giovangigli, V., and Nandula, S. P., "The Structure of Nonpremixed Hydrogen-Air Flames," *Combust. Sci. and Tech.* **104** (1995), pp 427–439.

9. Ilincic, N., Bui-Pham, M. N., and Seshadri, K., "Structure of Nonpremixed CH_4/NO_2 Flames," submitted for publication in Combustion Science and Technology, December 1995.

10. Anderson, W. R., Ilincic, N., and Seshadri, K., "Studies of Reactions Pertaining to and Development of a Reduced Mechanism for the Double Base Propellant Dark Zone," To appear in the proceedings of the 31st JANNAF Combustion Meeting, Sunnyvale, CA, October, 1994.

1.2.2 Ph.D Theses

The Ph.D theses completed using support from this research program are

1. Mary N. Bui-Pham, "Studies in Structures of laminar Hydrocarbon Flames," Ph.D Thesis, University of California at san Diego, La Jolla, California, 1992.

2. Bo Yang, "The Structure of Methane, Methanol and Formaldehyde Flames," Ph.D Thesis, University of California at san Diego, La Jolla, California, 1993.

3. Nenad Ilincic, "Ignition and Extinction Phenomena in Combustion Systems," Ph.D Thesis, University of California at san Diego, La Jolla, California, 1995.

A significant part of the important results obtained in this study are summarized in the publications. Reprints of publications 1–8 and 10 are provided. Reprints of publication 9 will be provided as soon as they become available. A significant part of the results discussed in the Ph.D theses are also summarized in these publications. Chapter 2 summarizes results of our studies on the structure of nonpremixed CH_4/NO_2 flames which is also included in publication number 9. Chapter 3 summarizes results of our study on the structures of $CH_4/NO_2/O_2$ and $CH_2O/NO_2/O_2$ premixed flames which are not available in the publications and is taken from the thesis of Yang (1993).

Chapter 2

The Structure of Nonpremixed CH_4/NO_2 Flames

2.1 Introduction

There is interest in research on nitramine combustion because among energetic materials, nitramines possess many desirable qualities such as high specific impulse and stable combustion in propulsive systems where they are used and low levels of pollutants and smoke formed during combustion. These attributes have prompted many experimental and theoretical studies on the combustion of nitramines. The physical and chemical processes that govern the ignition and combustion of nitramine propellants are complex and involve decomposition of the propellant into several compounds and combustion of these compounds in stages. Kubota (1981) observed that the nitramine particles melt and diffuse into a melting binder on the burning surface of the propellant and generate a homogeneous mixture of reactive species. This homogeneous mixture then oxidizes in the gas phase. Melius (1988) identified, in the gas phase, a primary flame zone composed of a very endothermic pyrolysis region followed by a dark zone and a luminous secondary reaction zone. Previous numerical studies using detailed gas-phase chemistry have demonstrated the importance of the secondary reaction zone in controlling the burning rate of neat RDX (Melius 1986, Melius 1987, Melius 1988, Melius 1989). The success of these numerical studies illustrates the utility of fundamental approaches to clarify the combustion of nitramines.

The gas-phase combustion of nitramines takes place in a number of subsystems, and the reactions between CH_4-NO_2 and CH_2O-NO_2 are such subsystems. An improved understanding of the chemistry taking place in these systems can be useful in modeling the combustion of nitramines. Hydrocarbon compounds evolve from decomposition of the binder and CH_4 is chosen to represent these hydrocarbon compounds. In solid propellants where the fuel

and oxidizer are not premixed on the molecular level, they evolve separately and react in a nonpremixed configuration. For this reason numerical calculations are performed in CH_4-NO_2 systems. These calculations are performed using a detailed chemical-kinetic mechanism, a skeletal chemical-kinetic mechanism, a 10-step reduced chemical-kinetic mechanism and a 7-step reduced chemical-kinetic mechanism. The skeletal mechanism is deduced from the detailed mechanism after removing reactions which are found to have a negligible influence on the flame structure and critical conditions of extinction. The reduced mechanisms are derived from the skeletal mechanism.

As an initial step toward understanding gas-phase nitramine combustion, results of numerical calculations of the structure of counterflow, nonpremixed methane/nitrogen dioxide flame studies are discussed for various values of pressure. The primary issue addressed in this work is the influence of strain on the structure and extinction of these flames for a pressure range from 1 to 10 atm. Although experimental studies on premixed flames burning $CH_4/NO_2/O_2$ mixtures are available (Branch, Sadeqi, Alfarayedhi & Tiggelen 1991, Zabarnick 1991), similar experimental studies on nonpremixed CH_4/NO_2 flames have not yet been conducted.

2.2 Detailed Chemical Kinetic Mechanism and Numerical Formulation

A detailed chemical-kinetic mechanism comprising 137 elementary reactions among 33 species shown in Table 2.1 is used to describe the structure of CH_4/NO_2 flames. All elementary reactions are presumed to be reversible. For each elementary reaction n, Table 2.1 shows the values of the frequency factor A_n, the temperature exponent b_n, and the activation energy E_n that appear in the parametric expression $k_n = A_n T^{b_n} \exp[-E_n/(\hat{R}T]$ for the specific reaction rate constant k_n. Here $\hat{R}$ represents the universal gas constant and T the gas temperature. This mechanism is deduced from the comprehensive mechanism of Miller & Bowman (1989) by including reactions appropriate to CH_4/NO_2 systems. The mechanism of Miller & Bowman (1989) was developed to describe the gas phase reactions of nitrogen compounds that are required to predict the formation of air pollutants. This mechanism (Miller & Bowman 1989) did not include some reactions which could be important is systems where NO_2 and NO are present in large quantities such as those considered here. To make up for this exclusion reactions 132–137 taken from Zabarnick (1991) are included in the detailed mechanism. The elementary reaction 1 taken from Smooke & Giovangigli (1991a) is also included in the detailed mechanism because this reaction is found to influence the critical conditions of extinction of methane-air flames.

In developing the chemical-kinetic mechanism reactions which include species comprising two or more carbon atoms are neglected. This approximation is consistent with previous numerical studies on the structure of nonpremixed methane-air flames (Smooke, Puri & Seshadri 1986, Chelliah, Law, Ueda, Smooke & Williams 1990, Smooke & Giovangigli 1991a, Smooke & Giovangigli 1991b, Chelliah, Seshadri & Law 1993). In nonpremixed CH_4/NO_2 flames it could be assumed that species comprising two or more carbon compounds are formed on the fuel side of the flame as in methane-air flames, following the pyrolysis of methane and the formation of methyl radicals. However, numerous previous studies that provided valuable insight on methane-air flames restricted the chemical kinetic representation to include only C_1 chemistry (by neglecting reactions with species comprising two or more carbon compounds). The flame structure and critical conditions of extinction calculated using this simplified representation were in good agreement with measurements (Smooke et al. 1986, Chelliah et al. 1990). Furthermore Zabarnick (1991) cited the lack of high-temperature kinetic data for the reactions of NO_2 with hydrocarbon species as a probable cause for the disagreement between modeling and experimental results of $CH_4/NO_2/O_2$ premixed flames. This work by Zabarnick (1991) used the chemical-kinetic mechanism of Miller & Bowman (1989) as the base mechanism. Indeed, there appears to be scarce high temperature data (above 600 K) for the reactions among species comprising two or more carbon atoms and nitrogen compounds.

These observations suggest that either the the chemical reactions taking place on the fuel side of nonpremixed CH_4/NO_2 flames is similar to those on the fuel side of nonpremixed methane/air flame, or, less likely, that if they were different, the reactions and their rates are not known with sufficient accuracy. Therefore the chemical-kinetic mechanism employed here includes only C_1 chemistry.

Numerical calculations are performed to determine the structure and critical conditions of extinction of diffusion flames stabilized between two counterflowing streams, one containing methane and the other containing nitrogen dioxide. The ambient reactant stream containing the fuel is presumed to flow toward the stagnation plane from $y = -\infty$, and the ambient reactant stream containing nitrogen dioxide is presumed to flow toward the stagnation plane from $y = \infty$. Here y represents the spatial coordinate normal to the surface of the flame. Smooke & Giovangigli (1991a) have summarized the conservation equations for mass, momentum and energy, and the balance equation for species which are used here to describe the flame structure. In configurations where the external flow is inviscid and irrotational, a parameter reflecting the fluid dynamic environment can be taken to be the strain rate exerted on the flame by the external oxidizer stream $K_O \equiv (-dv_y/dy)_\infty = ja_\infty$ where v_y represents the velocity component normal to the surface of the flame, and the subscript ∞ denotes conditions in the external, ambient NO_2-stream. The quantity $j = 1$ for planar flow and $j = 2$

for axisymmetric flow and $a_\infty = (dv_x/dx)_\infty$, where v_x and x represent the velocity component and spatial coordinate parallel to the surface of flame respectively.

The numerical calculations can be performed employing either the "potential–flow" or the "plug-flow" boundary conditions. If the outer flow is inviscid and irrotational then potential-flow boundary conditions must be used. For potential flow, on each side of the stagnation plane the value of dv_x/dx is independent of y, and at the ambient nitrogen dioxide stream $v_x/(a_\infty x) = 1.0$, and at the ambient fuel stream $v_x/(a_\infty x) = \sqrt{\rho_\infty/\rho_{-\infty}}$, where ρ is the gas density and the subscript $-\infty$ denotes conditions in the external, ambient fuel stream. Also for these potential flow boundary conditions the stagnation plane is located at $y = 0$, where $v_y = 0$. It is well known that "plug-flow" boundary conditions must be used if the results of numerical calculations are to be compared with experimental measurements (Seshadri & Williams 1978, Chelliah et al. 1990, Trees, Brown, Seshadri, Smooke, Balakrishnan, Pitz, Giovangigli & Nandula 1995, Grudno & Seshadri 1995). In the plug-flow approximation $v_x = 0$ at the exit of the ducts from which the reactants are introduced into the flow-field. Seshadri & Williams (1978) have shown that for plug-flow, if the Reynolds number at the exit of the duct is sufficiently large, then two inviscid and rotational flow regions separated by a thin viscous region will be formed. Also, in the plug-flow configuration dv_x/dx is a function of y and Seshadri & Williams (1978) have deduced expressions for calculating the value of dv_x/dx at the stagnation plane. Since the focus of this paper is to clarify the influence of strain on the structure and critical conditions of extinction of nonpremixed CH_4/NO_2 flames, and is not concerned with comparing results of numerical calculations with measurements, calculations are performed employing potential flow boundary conditions for flames stabilized in planar flows.

Numerical calculations are performed with the values of the mass fractions of methane and nitrogen dioxide in the ambient streams set equal to unity and the value of the temperature set equal to 330 K. The value of a_∞ is also specified. Calculations are performed for values of pressure p equal to 1, 2, and 10 atmospheres.

2.3 Flame Structure

Figures 2.1, 2.2, and 2.3 show profiles of temperature and the mole fraction of major species, some intermediate species, and some radicals calculated using the detailed chemical-kinetic mechanism for $a_\infty = 60\ s^{-1}$ and $p = 1$ atm. The profiles in Figures 2.1, 2.2, and 2.3 are plotted as functions of the mixture fraction $Z = Z_C/Z_{C,F}$, where Z_C is the mass fraction of element carbon and $Z_{C,F}$ is the value of Z_C at the ambient fuel stream. It follows from this definition that $Z = 0$ in the ambient NO_2 stream and $Z = 1.0$ in the ambient fuel stream.

The mass fraction of carbon is calculated from the relation $Z_C = \sum_{i=1}^{N} a_i Y_i W_C / W_i$ where W_C and W_i are respectively the molecular weight of carbon and species i, Y_i is the mass fraction of species i, a_i is the number of carbon atoms in a molecule of species i, and N is the total number of species.

In Fig. 2.1 the profiles of the temperature T of the reactants CH_4 and NO_2 and the major products CO_2, H_2O and N_2 are plotted. The temperature profile in Fig. 2.1 shows that chemical reactions are taking place in a broad zone in comparison to those in nonpremixed methane-air flames (Smooke et al. 1986). The fuel and nitrogen dioxide are consumed in two different regions of the flame. The peak values of the products CO_2, H_2O, and N_2 are attained between the regions where CH_4 and NO_2 are consumed. Figure 2.2 shows profiles of the intermediate species O_2, H_2, CO, NO, and HCN. The peak values of the intermediate species H_2, and CO are attained at the region where CH_4 is consumed and the peak values of O_2 and NO are attained at the region where NO_2 is consumed. Figure 2.2 shows the peak value of HCN is reached at the position where CH_4 is consumed. Figure 2.3 shows profiles of the radicals OH, H, O, and N. After comparing the profiles in Figures 2.1, 2.2, and 2.3 it can be observed that the peak values of the radicals OH, H, O and N are reached between the regions where CH_4 and NO_2 are consumed. Also these radicals are consumed in the regions where CH_4 and NO_2 are consumed.

The profiles in Figures 2.1, 2.2, and 2.3 is used to divide the zone where chemical reactions are taking place into three regions—a fuel-consumption region, a NO_2-consumption region and a product-formation region. In the fuel-consumption region the predominant reactions taking place are those between the fuel and the radicals to form the intermediate compounds H_2 and CO. In the NO_2-consumption region the predominant reactions are between the NO_2 and radicals to form the intermediate compounds NO and O_2. In the product-formation region the products CO_2, H_2O and N_2 are formed from the intermediate species. The radicals are also formed in the product-formation region. The asymptotic structure of the fuel-consumption region and the product-formation region appears to be similar to the structure of these zones in methane-air flames (Seshadri & Williams 1994). These observations are used to derive the reduced chemical-kinetic mechanism.

2.4 Skeletal and Reduced Chemical Kinetic Mechanisms

A skeletal chemical-kinetic mechanism is derived from the detailed chemical-kinetic mechanism after removing species and reactions which have a negligible influence on the critical conditions of extinction. All elementary reactions in which the species CH_3O, H_2O_2, NH, H_2CN, NNH, C_2N_2, HOCN, and HNCO participate are removed. In addition the elementary

steps 132–137 are also removed. The skeletal mechanism comprises reactions 1–92 shown in Table 2.1. Twenty-five species are present in the skeletal mechanism. If reactions in which HCN and HCNO participate are removed, then the value of of extinction strain rate is approximately 5 times lower than its calcualted value with these reactions included in the mechanism.

Procedures for deriving reduced chemical-kinetic mechanisms are described in detail elsewhere (Peters 1991). Since the skeletal mechanism is made up of 25 reactive species and four chemical elements, twenty-one independent species balance equations can be written (Seshadri & Williams 1994). Therefore the skeletal mechanism is equivalent to a reduced chemical-kinetic mechanism having 21 overall steps. To identify species for which steady-state approximations can be introduced, the magnitudes of the various terms in the balance equation for each intermediate species were plotted as a function of Z using the results of numerical calculations with the skeletal mechanism. Steady-state approximations are introduced for those species for which the absolute values of the chemical production rates and destruction rates are much larger than the absolute values of the other terms in the balance equation (Williams 1985). Using this procedure, the results of the numerical calculations show that it is reasonable to introduce steady-state approximation for the eleven species HO_2, CH_2O, HCO, CH_2, CH, CN, N, HCNO, HNO, N_2O, and NCO appearing in the skeletal chemical-kinetic mechanism. The reduced chemical-kinetic mechanism now comprises ten overall steps which can be written as

$$\begin{aligned}
CH_4 + H &\rightleftharpoons CH_3 + H_2 && \text{I}\\
CH_3 + O &\rightleftharpoons H + H_2 + CO, && \text{II}\\
H + H + M &\rightleftharpoons H_2 + M, && \text{III}\\
OH + CO &\rightleftharpoons H + CO_2, && \text{IV}\\
H + O_2 &\rightleftharpoons OH + O, && \text{V}\\
H + NO_2 &\rightleftharpoons OH + NO, && \text{VI}\\
NO + NO &\rightleftharpoons O_2 + N_2, && \text{VII}\\
H_2 + OH &\rightleftharpoons H + H_2O, && \text{VIII}\\
H_2 + O &\rightleftharpoons H + OH, && \text{IX}\\
HCN + NO + O_2 + H &\rightleftharpoons H_2 + 2\,O + CO + N_2, && \text{X}
\end{aligned}$$

The rates of the overall steps w_k, k = I–X expressed in terms of the rates of the elementary

reactions w_n, n = 1–92 are

$$\left.\begin{aligned}
w_I &= -w_1 + w_2 + w_3 + w_4, \\
w_{II} &= w_5 + w_{49} + w_{59} + w_{72}, \\
w_{III} &= w_1 - w_8 + w_{10} + w_{12} + w_{13} + w_{14} + w_{15} + w_{16} + \\
&\quad w_{24} + w_{29} + w_{30} + w_{31} + w_{32} + w_{33} + w_{34} + w_{35} - \\
&\quad w_{41} + w_{52} + w_{55} + w_{56} + w_{63} + w_{67} + w_{68} + w_{70} + \\
&\quad w_{71} + w_{78} + w_{83} + w_{84} + w_{85} + w_{90} + w_{91} \\
w_{IV} &= w_{14} + w_{16} + w_{17} + w_{18} + w_{19} - w_{37} - w_{50} + w_{53} + w_{55} - w_{65}, \\
w_V &= w_{18} + w_{19} + w_{20} - w_{22} + w_{26} - w_{35} - w_{37} + w_{38} - w_{40} - \\
&\quad w_{44} + w_{45} + w_{46} + w_{48} + w_{53} + w_{54} + w_{55} + w_{56} + w_{57} + \\
&\quad w_{58} + w_{62} - w_{67} - w_{70} - w_{71} + w_{72} + w_{74} + w_{75} + w_{76} - \\
&\quad w_{77} - w_{78} - w_{81} - w_{82} - w_{83} - w_{84} - w_{85} - w_{86}, \\
w_{VI} &= -w_{38} + w_{39} + w_{40} + w_{41} + w_{82}, \\
w_{VII} &= -w_{37} - w_{43} - w_{44} + w_{45} + w_{46} + w_{48} - \\
&\quad w_{71} + w_{72} - w_{84} - w_{85} - w_{86} \\
w_{VIII} &= w_4 + w_6 + w_{10} + w_{21} + w_{25} + w_{28} + w_{33} + w_{50} + w_{51} + w_{52} + \\
&\quad w_{53} + w_{54} + w_{55} + 2w_{56} + w_{57} + w_{58} - w_{59} + w_{60} + w_{61} + w_{62} + \\
&\quad w_{63} + w_{64} + w_{65} + w_{74} + 2w_{75} + w_{76} - w_{77} + w_{79} + w_{90}, \\
w_{IX} &= w_2 + w_9 + w_{13} + w_{14} + w_{15} + w_{16} + w_{20} + w_{23} + w_{24} - w_{25} - \\
&\quad w_{28} + w_{34} + w_{35} - w_{36} - w_{41} - w_{45} - w_{46} - w_{49} + w_{51} + w_{52} + \\
&\quad w_{53} + w_{55} + w_{56} + w_{57} + w_{58} - w_{59} + w_{63} + w_{67} + w_{68} + w_{70} + \\
&\quad w_{71} - w_{72} + w_{76} + w_{78} + w_{79} + w_{83} + w_{84} + w_{85}, \\
w_X &= -w_{45} - w_{46} - w_{48} - w_{72} - w_{73} + w_{75} + w_{76} - w_{77} + w_{79}.
\end{aligned}\right\} \quad (2.1)$$

To further simplify the mechanism, steady-state assumptions are introduced for the species OH, O, and HCN which gives seven overall steps which can be written as

$$\begin{aligned}
\mathrm{CH_4 + H} &\rightleftharpoons \mathrm{CH_3 + H_2} && \mathrm{I^s} \\
\mathrm{CH_3 + H + H_2O} &\rightleftharpoons \mathrm{3\ H_2 + CO}, && \mathrm{II^s} \\
\mathrm{H + H + M} &\rightleftharpoons \mathrm{H_2 + M}, && \mathrm{III^s} \\
\mathrm{H_2O + CO} &\rightleftharpoons \mathrm{H_2 + CO_2}, && \mathrm{IV^s} \\
\mathrm{3\ H_2 + O_2} &\rightleftharpoons \mathrm{2\ H + 2\ H_2O}, && \mathrm{V^s} \\
\mathrm{H_2 + NO_2} &\rightleftharpoons \mathrm{H_2O + NO}, && \mathrm{VI^s} \\
\mathrm{NO + NO} &\rightleftharpoons \mathrm{O_2 + N_2}, && \mathrm{VII^s}
\end{aligned}$$

The rates of the overall steps of the seven step mechanism w_k, k = $\mathrm{I^s}$–$\mathrm{VII^s}$ are respectively identical to the rates for the overall steps I–VII for the ten-step mechanism shown in Eq. 2.1. The structure and critical conditions of flame extinction are calculated numerically using the skeletal mechanism and the reduced chemical-kinetic mechanisms. The results are discussed in the next section.

2.5 Results and Discussions

Figures 2.4, 2.5, 2.6, 2.7, and 2.8 show profiles of temperature and the mole fraction of reactants, products, intermediate species and radicals calculated using the detailed chemical-kinetic mechanism (solid line), skeletal chemical-kinetic mechanism (dashed line), reduced 10-step mechanism (chain line), and reduced 7-step mechanism (dotted line) for $a_\infty = 350\ s^{-1}$ and $p = 1$ atm. Figures 2.4, and 2.5 show that the profiles of T, CH_4, NO_2, CO_2, H_2O and N_2 calculated using the skeletal mechanism and the reduced 10-step mechanism agree well with those calculated using the detailed mechanism. The peak value of the temperature profile calculated using the reduced 7-step mechanism is lower than those calculated using the other mechanisms and it is reached at a smaller value of Z. The profile of the mole fraction of the reactant NO_2 calculated using the 7-step mechanism show that this compound is consumed at a lower value of Z in comparison to those calculated using the other mechanisms. Also the profile of N_2 calculated using the reduced 7-step mechanism deviates from those calculated using the other mechanisms. This is attributed to inaccuracies associated with steady-state approximations for OH, O, and HCN.

Figure 2.6 shows the profiles of the intermediate species NO, O_2, CO and H_2 calculated using the skeletal mechanism and the reduced 10-step mechanism to agree well with those calculated using the detailed mechanism. The profiles of CO and H_2 calculated using the reduced 7-step mechanism agrees reasonably well with those calculated using the other mechanisms. The peak values of NO and O_2 calculated using the reduced 7-step mechanism is higher than those calculated using the other mechanisms and it is reached at a smaller value of Z. The shift in the locations of the peak values of NO and O_2 are consistent with the shift in the location of the region where NO_2 is consumed as shown in Fig. 2.4. Figures 2.7, and 2.8 show profiles of the radicals H, OH and O. The peak values of these radicals calculated using the skeletal and reduced 10-step mechanism are in reasonably good agreement. The peak values of the radicals calculated using the reduced 7-step mechanism are significantly higher than those calculated using the skeletal mechanism and the reduced 10-step mechanism. The qualitative features of the flame structure shown in the profiles in Figs. 2.4, 2.5, 2.6, 2.7, and 2.8 are similar to those shown in Figs. 2.1, 2.2, and 2.3. These figures show the chemical reactions to take place in three regions—the fuel-consumption region, the NO_2-consumption region and the product-formation region.

The detailed skeletal and reduced chemical-kinetic mechanisms are used to calculate the critical conditions of flame extinction. The flame structure is calculated for various values of the strain rate. The critical value of the strain rate at extinction is defined as that value beyond which a converged solution is not obtained. Table 2.2 shows the values of the critical conditions of extinction calculated using the various mechanisms for $p = 1, 2$, and 10 atm. The

values of a_∞ calculated using the various mechanisms are in good agreement. All mechanisms show the critical strain rate at extinction to increase with increasing values of p.

In deducing the reduced 7-step mechanism from the reduced 10-step mechanism steady-state approximations were introduced for the species O, OH, and HCN. The peak values of the flame temperature and the values of the critical conditions of flame extinction are found not to be influenced by introducing steady-state approximation for O. The peak values of the flame temperature and the values of the critical conditions of flame extinction are found to increase if steady-state approximation is introduced for OH and the values of these quantities are found to decrease if steady-state approximation is introduced for HCN.

2.6 Summary and Conclusions

Numerical calculations are performed using a detailed, skeletal, reduced 10-step and a reduced 7-step mechanism to calculate the structure and critical conditions of extinction of nonpremixed CH_4/NO_2 flames. The flame structure calculated using the skeletal mechanism and reduced 10-step mechanism agree well with those calculated using the detailed mechanism. The peak values of the temperature and mole fraction of the radicals calculated using the reduced 7-step mechanism are reached slightly at a smaller value of Z than those calculated using the other mechanisms. The critical conditions of flame extinction calculated using the various mechanisms agree reasonably well with each other. The differences in the values of the the strain rate at extinction calculated using the detailed mechanism and skeletal mechanism are less than 4%, those between the skeletal mechanism and the reduced 10-step mechanism and between the the reduced 10-step and 7-step mechanisms are less than 12 %.

Table 2.1: Detailed and Skeletal Chemical-Kinetic Mechanisms and Associated Rate Constants.

	Reactions		A_n	b_n	E_n
1.	$CH_3+H+M=CH_4+M$	k_∞	2.11E+14	0.0	0.0
		k_0	6.26E+23	-1.80	0.0
	/H_2 2.0/CO 2.0/CO_2 3.0/H_2O 5.0/				
2.	$CH_4+O_2=CH_3+HO_2$		7.90E+13	0.0	56000.0
3.	$CH_4+H=CH_3+H_2$		2.20E+04	3.0	8750.0
4.	$CH_4+OH=CH_3+H_2O$		1.60E+06	2.1	2460.0
5.	$CH_3+O=CH_2O+H$		8.00E+13	0.0	0.0
6.	$CH_2O+OH=HCO+H_2O$		3.43E+09	1.2	-447.0
7.	$CH_2O+H=HCO+H_2$		2.19E+08	1.8	3000.0
8.	$CH_2O+M=HCO+H+M$		3.31E+16	0.0	81000.0
9.	$CH_2O+O=HCO+OH$		1.80E+13	0.0	3080.0
10.	$HCO+OH=H_2O+CO$		1.00E+14	0.0	0.0
11.	$HCO+M=H+CO+M$		2.50E+14	0.0	16802.0
	/CO 1.9/H_2 1.9/CH_4 2.8/CO_2 3.0/H_2O 5.0/				
12.	$HCO+H=CO+H_2$		1.19E+13	0.2	0.0
13.	$HCO+O=CO+OH$		3.00E+13	0.0	0.0
14.	$HCO+O=CO_2+H$		3.00E+13	0.0	0.0
15.	$HCO+O_2=HO_2+CO$		3.30E+13	-0.4	0.0
16.	$CO+O+M=CO_2+M$		6.17E+14	0.0	3000.0
17.	$CO+OH=CO_2+H$		1.51E+07	1.3	-758.0
18.	$CO+O_2=CO_2+O$		1.60E+13	0.0	41000.0
19.	$HO_2+CO=CO_2+OH$		5.80E+13	0.0	22934.0
20.	$H_2+O_2=2OH$		1.70E+13	0.0	47780.0
21.	$OH+H_2=H_2O+H$		1.17E+09	1.3	3626.0
22.	$O+OH=O_2+H$		4.00E+14	-0.5	0.0
23.	$O+H_2=OH+H$		5.06E+04	2.7	6290.0
24.	$H+O_2+M=HO_2+M$		3.61E+17	-0.7	0.0
	/CO 2.1/H_2 2.9/CO_2 4.2/H_2O 1.86/N_2 1.3/				
25.	$OH+HO_2=H_2O+O_2$		7.50E+12	0.0	0.0
26.	$H+HO_2=2OH$		1.40E+14	0.0	1073.0
27.	$O+HO_2=O_2+OH$		1.40E+13	0.0	1073.0
28.	$2OH=O+H_2O$		6.00E+08	1.3	0.0
29.	$2H+M=H_2+M$		1.00E+18	-1.0	0.0
	/H_2 0.0/CO_2 0.0/H_2O 0.0/				
30.	$2H+H_2=2H_2$		9.20E+16	-0.6	0.0
31.	$2H+H_2O=H_2+H_2O$		6.00E+19	-1.2	0.0
32.	$2H+CO_2=H_2+CO_2$		5.49E+20	-2.0	0.0
33.	$H+OH+M=H_2O+M$		1.60E+22	-2.0	0.0
	/H_2O 5.0/				
34.	$H+O+M=OH+M$		6.20E+16	-0.6	0.0
	/H_2O 5.0/				
35.	$2O+M=O_2+M$		1.89E+13	0.0	-1788.0
36.	$H+HO_2=H_2+O_2$		1.25E+13	0.0	0.0
37.	$CO_2+N=NO+CO$		1.90E+11	0.0	3400.0
38.	$HO_2+NO=NO_2+OH$		2.11E+12	0.0	-479.0
39.	$NO_2+H=NO+OH$		3.50E+14	0.0	1500.0
40.	$NO_2+O=NO+O_2$		1.00E+13	0.0	600.0
41.	$NO_2+M=NO+O+M$		1.10E+16	0.0	66000.0
42.	$N+NO=N_2+O$		3.27E+12	0.3	0.0
43.	$N+O_2=NO+O$		6.40E+09	1.0	6280.0
44.	$N+OH=NO+H$		3.80E+13	0.0	0.0
45.	$CH+N_2=HCN+N$		2.00E+11	0.0	13600.0
46.	$CH+NO=HCN+O$		1.10E+14	0.0	0.0

47.	$CH_2+H=CH+H_2$	1.00E+18	-1.6	0.0
48.	$CH_2+NO=HCNO+H$	1.39E+12	0.0	-1100.0
49.	$CH_3+OH=CH_2+H_2O$	7.50E+06	2.0	5000.0
50.	$CH_2+CO_2=CH_2O+CO$	1.10E+11	0.0	1000.0
51.	$CH_2+O=CO+2H$	5.00E+13	0.0	0.0
52.	$CH_2+O=CO+H_2$	3.00E+13	0.0	0.0
53.	$CH_2+O_2=CO_2+2H$	1.60E+12	0.0	1000.0
54.	$CH_2+O_2=CH_2O+O$	5.00E+13	0.0	9000.0
55.	$CH_2+O_2=CO_2+H_2$	6.90E+11	0.0	500.0
56.	$CH_2+O_2=CO+H_2O$	1.90E+10	0.0	-1000.0
57.	$CH_2+O_2=CO+OH+H$	8.60E+10	0.0	-500.0
58.	$CH_2+O_2=HCO+OH$	4.30E+10	0.0	-500.0
59.	$CH_3+H=CH_2+H_2$	9.00E+13	0.0	15100.0
60.	$CH_2+OH=CH+H_2O$	1.13E+07	2.0	3000.0
61.	$CH_2+OH=CH_2O+H$	2.50E+13	0.0	0.0
62.	$CH+O_2=HCO+O$	3.30E+13	0.0	0.0
63.	$CH+O=CO+H$	5.70E+13	0.0	0.0
64.	$CH+OH=HCO+H$	3.00E+13	0.0	0.0
65.	$CH+CO_2=HCO+CO$	3.40E+12	0.0	690.0
66.	$CH+H_2O=CH_2O+H$	4.57E+14	-0.8	0.0
67.	$N_2O+OH=N_2+HO_2$	2.00E+12	0.0	10000.0
68.	$N_2O+H=N_2+OH$	7.60E+13	0.0	15200.0
69.	$N_2O+M=N_2+O+M$	1.60E+14	0.0	51600.0
70.	$N_2O+O=N_2+O_2$	1.00E+14	0.0	28200.0
71.	$N_2O+O=2NO$	1.00E+14	0.0	28200.0
72.	$CH_3+NO=HCN+H_2O$	1.00E+11	0.0	15000.0
73.	$CH_2+N=HCN+H$	5.00E+13	0.0	0.0
74.	$CH+N=CN+H$	1.30E+13	0.0	0.0
75.	$HCN+OH=CN+H_2O$	1.45E+13	0.0	10929.0
76.	$HCN+O=CN+OH$	2.70E+09	1.6	29200.0
77.	$CN+H_2=HCN+H$	2.95E+05	2.5	2237.0
78.	$CN+O=CO+N$	1.80E+13	0.0	0.0
79.	$HCN+O=NCO+H$	1.38E+04	2.6	4980.0
80.	$CN+O_2=NCO+O$	5.60E+12	0.0	0.0
81.	$CN+OH=NCO+H$	6.00E+13	0.0	0.0
82.	$CN+NO_2=NCO+NO$	3.00E+13	0.0	0.0
83.	$CN+N_2O=NCO+N_2$	1.00E+13	0.0	0.0
84.	$NCO+O=NO+CO$	2.00E+13	0.0	0.0
85.	$NCO+N=N_2+CO$	2.00E+13	0.0	0.0
86.	$NCO+OH=NO+CO+H$	1.00E+13	0.0	0.0
87.	$NCO+M=N+CO+M$	3.10E+16	-0.5	48000.0
88.	$NCO+NO=N_2O+CO$	1.00E+13	0.0	-390.0
89.	$HNO+M=H+NO+M$	1.50E+16	0.0	48680.0
	$/H_2O$ 10.0/O_2 2.0/N_2 2.0/H_2 2.0/			
90.	$HNO+OH=NO+H_2O$	3.60E+13	0.0	0.0
91.	$HNO+H=H_2+NO$	5.00E+12	0.0	0.0
92.	$HCNO+H=HCN+OH$	1.00E+14	0.0	12000.0
93.	$CH_4+HO_2=CH_3+H_2O_2$	1.80E+11	0.0	18700.0
94.	$CH_3+HO_2=CH_3O+OH$	2.00E+13	0.0	0.0
95.	$CH_3+O_2=CH_3O+O$	2.05E+19	-1.6	29229.0
96.	$CH_3O+H=CH_3+OH$	1.00E+14	0.0	0.0
97.	$CH_3O+M=CH_2O+H+M$	1.00E+14	0.0	25000.0
98.	$CH_3O+H=CH_2O+H_2$	2.00E+13	0.0	0.0
99.	$CH_3O+OH=CH_2O+H_2O$	1.00E+13	0.0	0.0
100.	$CH_3O+O=CH_2O+OH$	1.00E+13	0.0	0.0
101.	$CH_3O+O_2=CH_2O+HO_2$	6.30E+10	0.0	2600.0

102.	$2HO_2=H_2O_2+O_2$	2.00E+12	0.0	0.0
103.	$H_2O_2+M=2OH+M$	1.30E+17	0.0	45500.0
104.	$H_2O_2+H=HO_2+H_2$	1.60E+12	0.0	3800.0
105.	$H_2O_2+OH=H_2O+HO_2$	1.00E+13	0.0	1800.0
106.	$CH_2+N_2=HCN+NH$	1.00E+13	0.0	74000.0
107.	$HCN+O=NH+CO$	3.45E+03	2.6	4980.0
108.	$NH+O_2=NO+OH$	7.60E+10	0.0	1530.0
109.	$NH+NO=N_2O+H$	2.40E+15	-0.8	0.0
110.	$NH+OH=N+H_2O$	5.00E+11	0.5	2000.0
111.	$NH+N=N_2+H$	3.00E+13	0.0	0.0
112.	$NH+H=N+H_2$	1.00E+14	0.0	0.0
113.	$NCO+H=NH+CO$	5.00E+13	0.0	0.0
114.	$H_2CN+N=N_2+CH_2$	2.00E+13	0.0	0.0
115.	$H_2CN+M=HCN+H+M$	3.00E+14	0.0	22000.0
116.	$CH_3+NO=H_2CN+OH$	1.00E+11	0.0	15000.0
117.	$CH_3+N=H_2CN+H$	3.00E+13	0.0	0.0
118.	$NNH+H=N_2+H_2$	1.00E+14	0.0	0.0
119.	$NNH+OH=N_2+H_2O$	5.00E+13	0.0	0.0
120.	$NNH+O=N_2O+H$	1.00E+14	0.0	0.0
121.	$NH+O_2=HNO+O$	1.00E+13	0.0	12000.0
122.	$NH+OH=HNO+H$	2.00E+13	0.0	0.0
123.	$NNH=N_2+H$	1.00E+14	0.0	0.0
124.	$NNH+NO=N_2+HNO$	5.00E+13	0.0	0.0
125.	$C_2N_2+O=NCO+CN$	4.57E+12	0.0	8880.0
126.	$C_2N_2+OH=HOCN+CN$	1.86E+11	0.0	2900.0
127.	$OH+HCN=HOCN+H$	5.85E+04	2.4	12500.0
128.	$OH+HCN=HNCO+H$	1.98E-03	4.0	1000.0
129.	$HOCN+H=HNCO+H$	1.00E+13	0.0	0.0
130.	$NCO+H_2=HNCO+H$	8.58E+12	0.0	9000.0
131.	$CN+HCN=C_2N_2+H$	2.00E+13	0.0	0.0
132.	$NO_2+NO_2=NO+NO+O_2$	2.00E+12	0.0	26825.0
133.	$NO_2+NO=N_2O+O_2$	1.00E+12	0.0	60000.0
134.	$NO+M=N+O+M$	4.00E+20	-1.5	150000.0
135.	$NO+NO=N_2+O_2$	1.30E+14	0.0	75630.0
136.	$NO+HNO=N_2O+OH$	2.00E+12	0.0	26000.0
137.	$NO+HO_2=HNO+O_2$	2.00E+11	0.0	2000.0

Table 2.2: Values of the critical strain rate at extinction a_∞ in s^{-1} calculated using the various mechanisms.

Mechanism	Extinction strain rate		
	1atm.	2atm.	10 atm.
Detailed	522	960	3810
Skeletal	502	935	3700
10-step	545	1040	3955
7-step	580	1170	4260

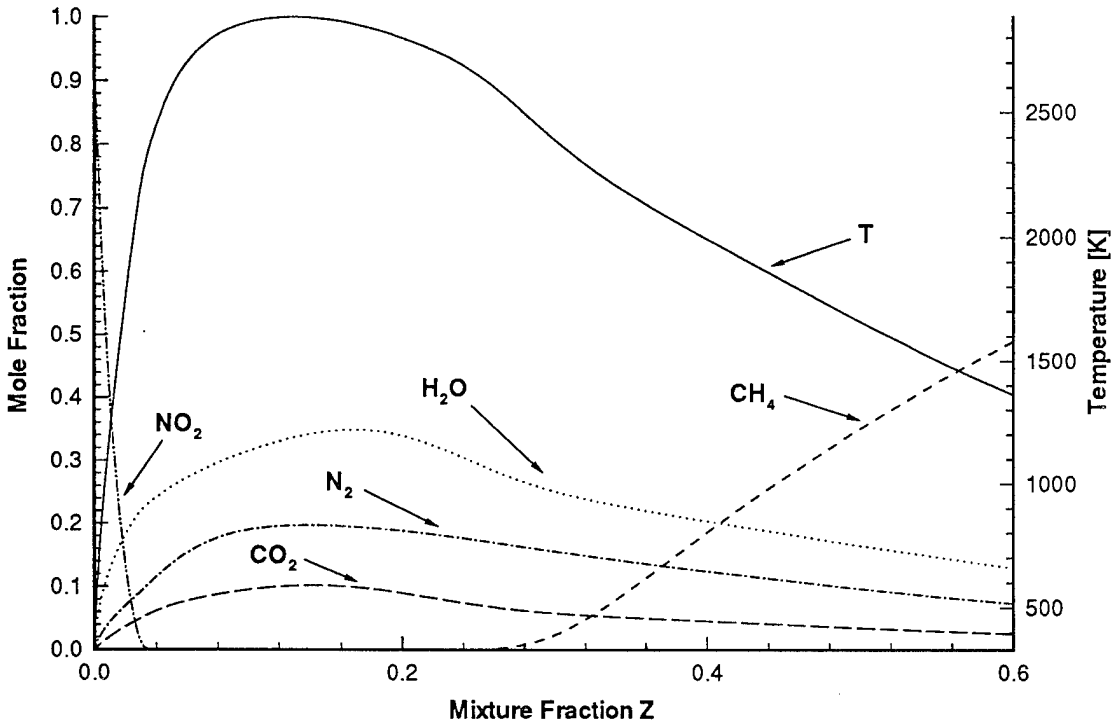

Figure 2.1: Profiles of temperature T and mole-fractions of major species—CH_4, NO_2, N_2, H_2O, and CO_2, calculated using the detailed chemical-kinetic mechanism for $a_\infty = 60\ s^{-1}$ and $p = 1$ atm.

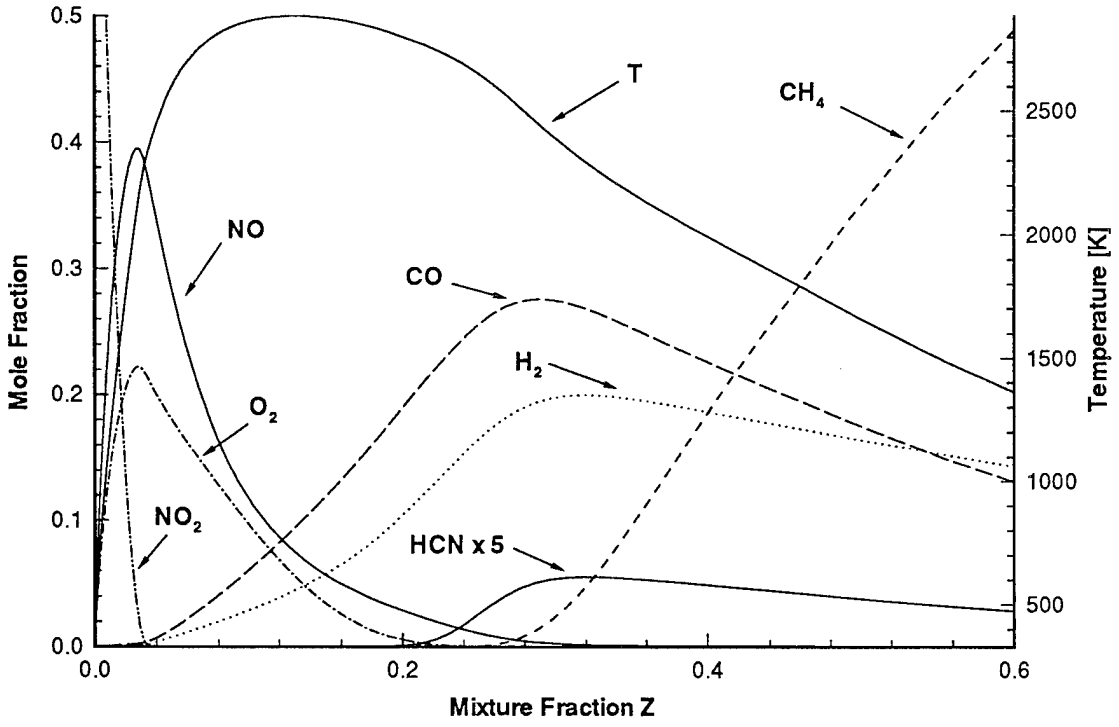

Figure 2.2: Profiles of temperature T and mole-fractions of CH_4 and NO_2 and the intermediate species—O_2, H_2, CO, NO, and HCN, calculated using the detailed chemical-kinetic mechanism for $a_\infty = 60\ s^{-1}$ and $p = 1$ atm.

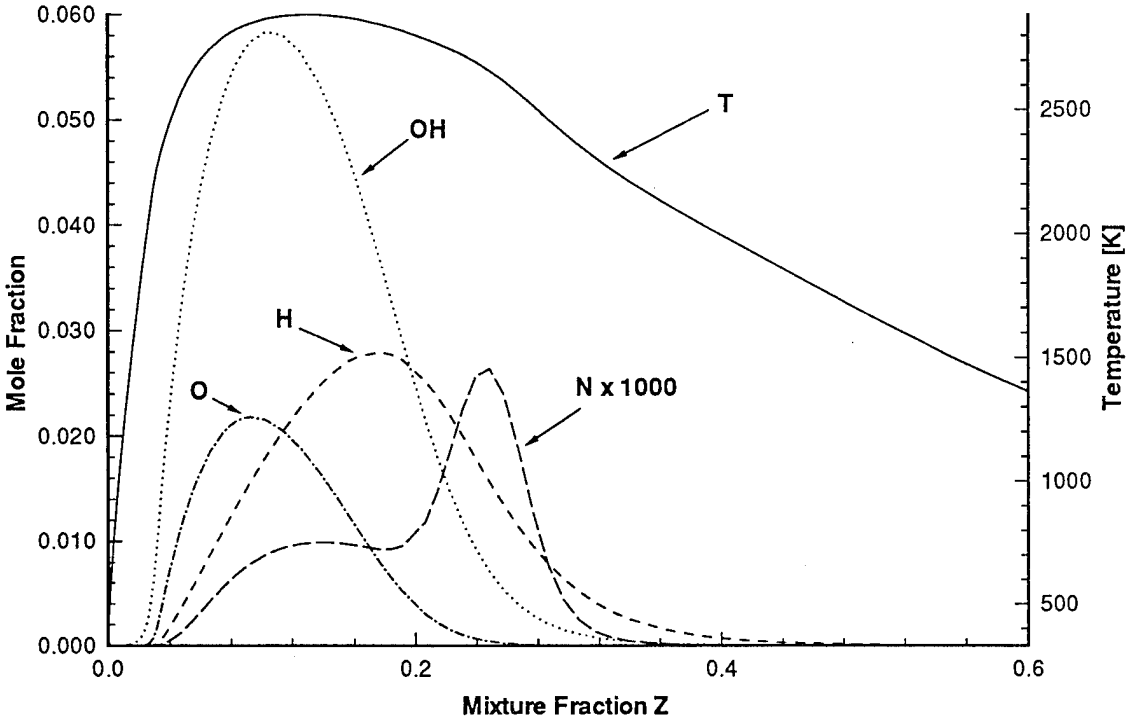

Figure 2.3: Profiles of temperature T and mole-fractions of the radicals—OH, H, O and N calculated using the detailed chemical-kinetic mechanism for $a_\infty = 60\ \mathrm{s}^{-1}$ and $p = 1$ atm.

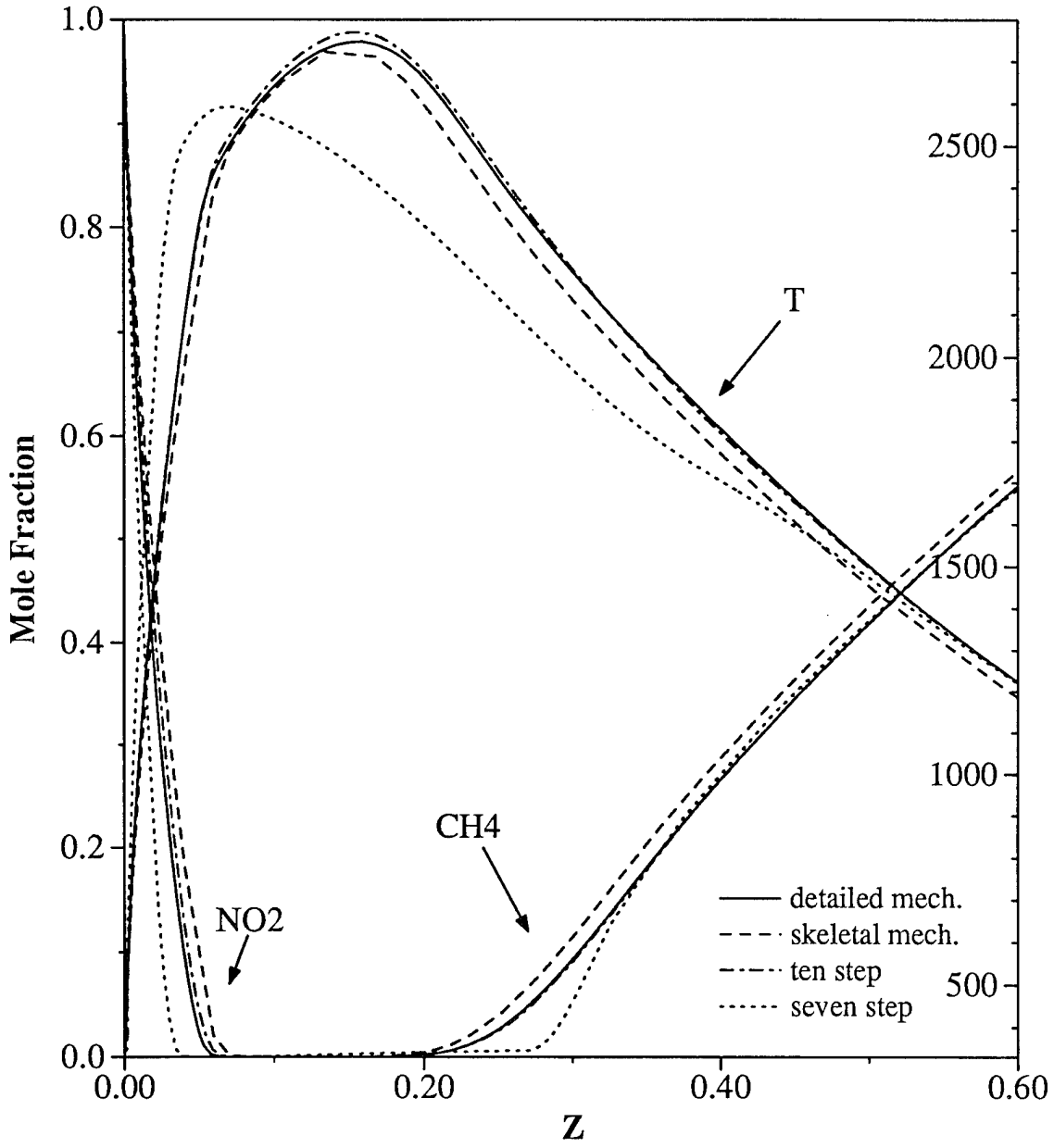

Figure 2.4: Profiles of temperature T and mole-fractions of the reactants CH_4, and NO_2 calculated using the detailed chemical-kinetic mechanism (solid line), skeletal chemical-kinetic mechanism (dashed line), reduced 10-step mechanism (chain line), and reduced 7-step mechanism (dotted line) for $a_\infty = 350\ s^{-1}$ and $p = 1$ atm.

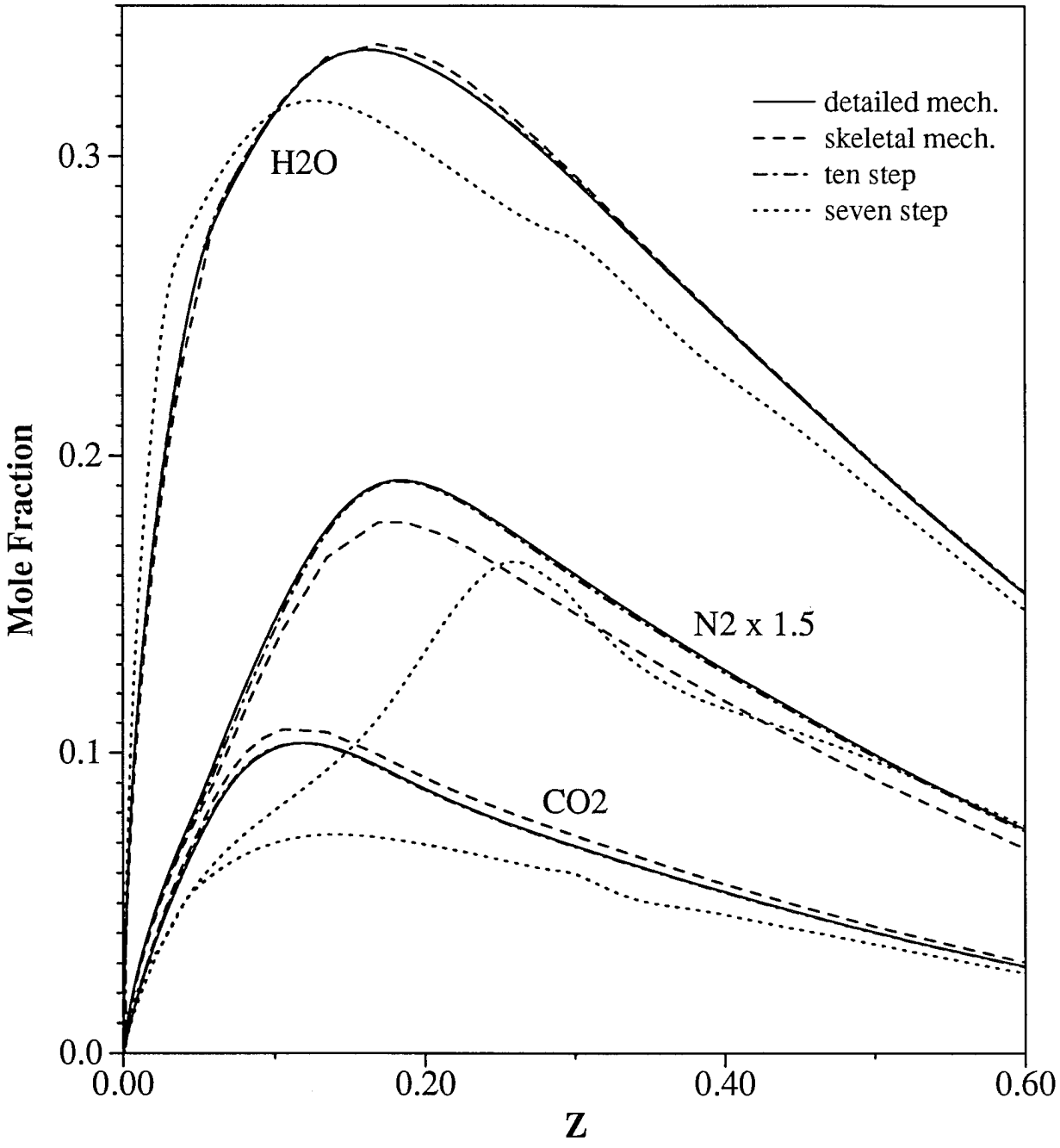

Figure 2.5: Profiles of mole-fractions of the products CO_2, H_2O, and N_2 calculated using the detailed chemical-kinetic mechanism (solid line), skeletal chemical-kinetic mechanism (dashed line), reduced 10-step mechanism (chain line), and reduced 7-step mechanism (dotted line) for $a_\infty = 350\ s^{-1}$ and $p = 1$ atm.

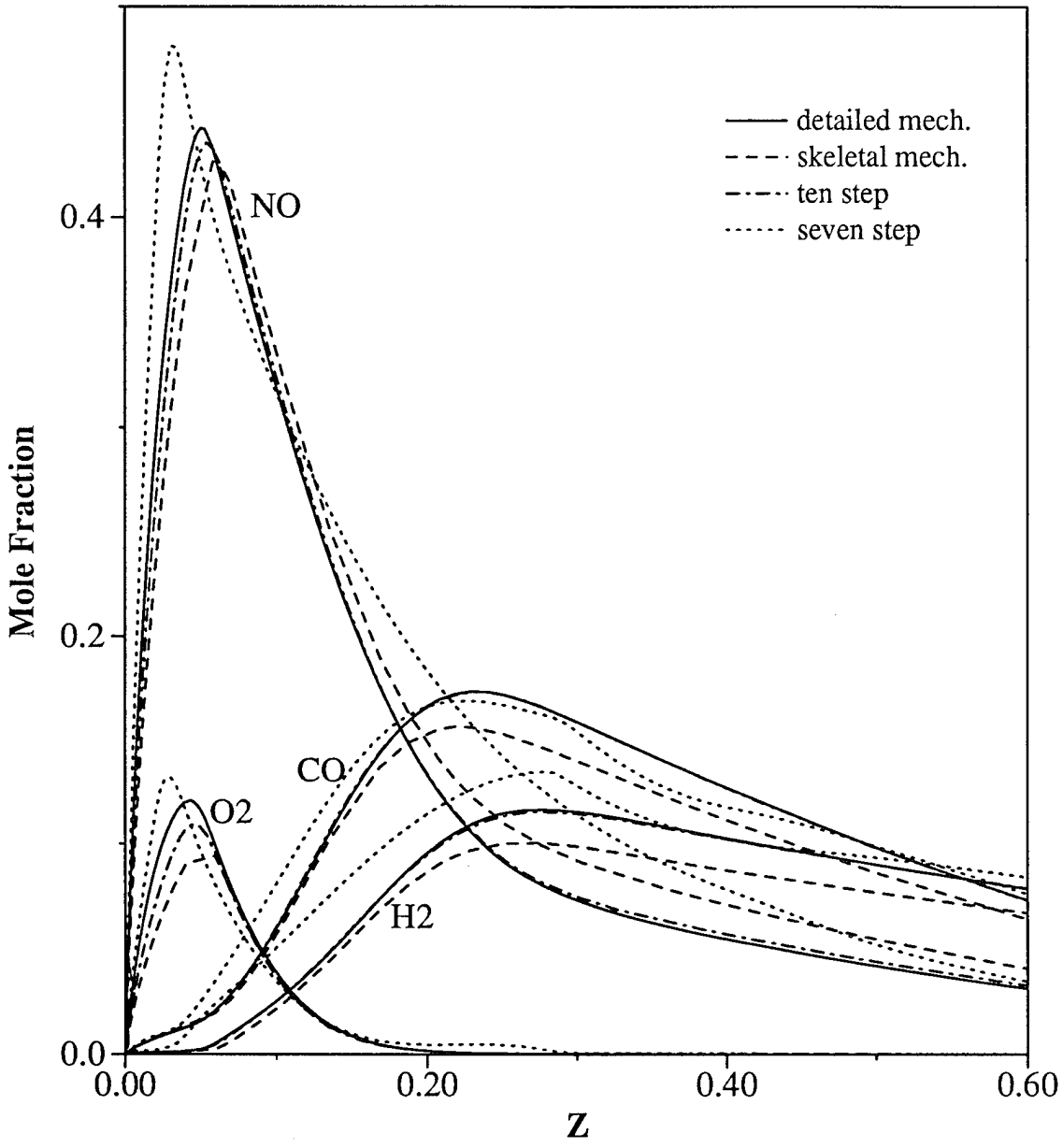

Figure 2.6: Profiles of mole-fractions of NO, O_2, CO, and H_2 calculated using the detailed chemical-kinetic mechanism (solid line), skeletal chemical-kinetic mechanism (dashed line), reduced 10-step mechanism (chain line), and reduced 7-step mechanism (dotted line) for a_∞ = 350 s^{-1} and p = 1 atm.

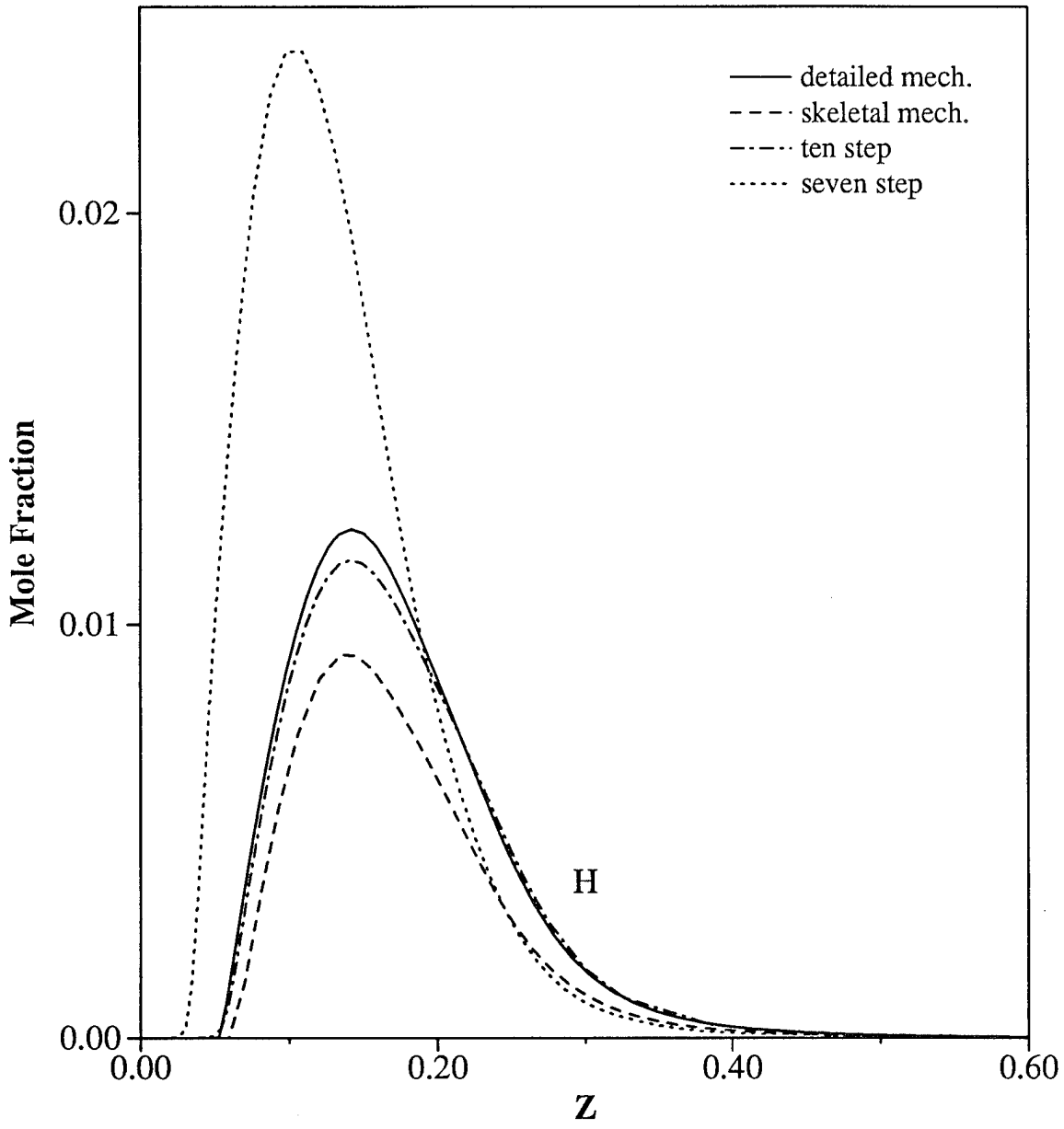

Figure 2.7: Profiles of mole-fractions of the radical H calculated using the detailed chemical-kinetic mechanism (solid line), skeletal chemical-kinetic mechanism (dashed line), reduced 10-step mechanism (chain line), and reduced 7-step mechanism (dotted line) for $a_\infty = 350\ \mathrm{s}^{-1}$ and $p = 1$ atm.

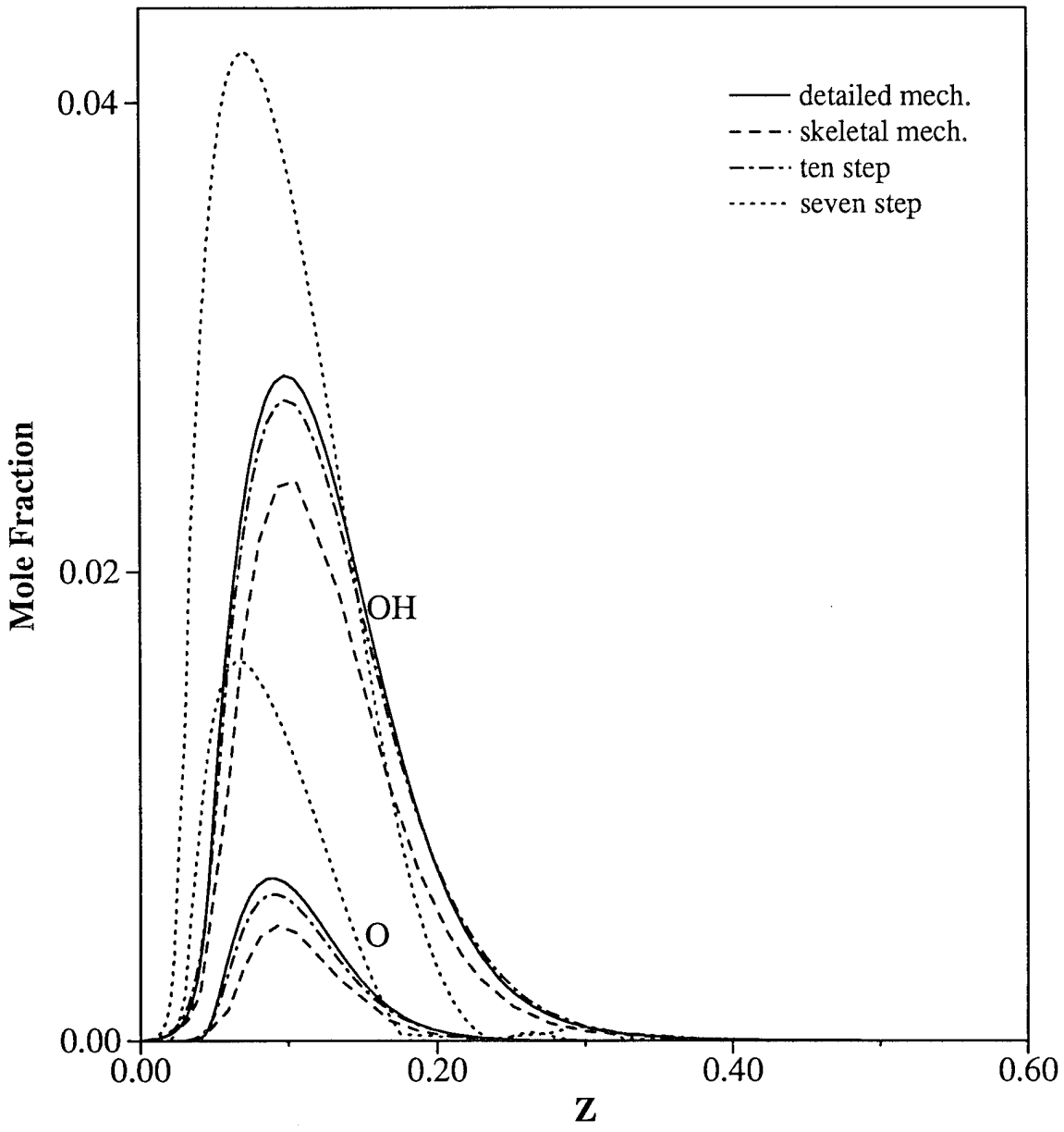

Figure 2.8: Profiles of mole-fractions of the radicals OH and O calculated using the detailed chemical-kinetic mechanism (solid line), skeletal chemical-kinetic mechanism (dashed line), reduced 10-step mechanism (chain line), and reduced 7-step mechanism (dotted line) for a_∞ = 350 s^{-1} and p = 1 atm.

Chapter 3

Structures of $CH_4/NO_2/O_2$ and $CH_2O/NO_2/O_2$ Premixed Flames

3.1 Introduction

This chapter is reproduced from Chapter 6 of the Ph.D thesis of Yang (1993).

Solid propellants such as nitramines used in rockets are complex compounds containing carbon, hydrogen, oxygen, and nitrogen. The combustion of solid propellants is a very complicated process that involves phase changes and chemical reactions, and in solid rocket engines, combustion occurs at very high pressure (Kuo & Summerfield 1984, Becker 1988). These unusual conditions and complexities make it difficult to study the structures of the flames experimentally and theoretically. Instead of directly studying solid propellant combustion, a more simple and fundamental way is to study the combustion of the species that are important in the combustion of solid propellants (Bui-Pham 1992, Sadeqi 1987, Branch et al. 1991, Zabarnick 1991). These simplified combustion systems should be able to maintain the characteristics of solid propellant flames. Since $CH_4/NO_2/O_2$ is a well studied flame and its reaction mechanism is relatively well established and, NO_2 and CH_2O are important species in the combustion of solid propellants, premixed $CH_4/NO_2/O_2$ and $CH_2O/NO_2/O_2$ flames are chosen here for investigation.

Branch et al. (1991) and Sadeqi & Branch (1991) studied $CH_4/NO_2/O_2$ and $CH_2O/NO_2/O_2$ premixed flames both experimentally and theoretically. The experiments (Branch et al. 1991, Sadeqi & Branch 1991) were done with laminar, premixed, flat flames under low pressures ($\approx$ 55 torr). Stable species were measured using quartz microprobe and gas chromatography. Temperatures were measured by thermocouples and Laser-Induced Fluorescence. It was found that NO_2 was just partially reacted in the flames, and pure CH_4/NO_2 flames could not be stabi-

lized but pure CH_2O/NO_2 flames could be stabilized. Zabarnick (1991) employed laser-induced fluorescence technique to study premixed $CH_4/NO_2/O_2$ flames at pressure of 55 torr. The chemical-kinetic processes of a burner-stabilized flame were also modeled (Zabarnick 1991), but difficulties were encountered in the modeling of a freely propagating flame with high starting concentrations of NO_2 (Zabarnick 1991).

Numerical calculations of $CH_4/NO_2/O_2$ diffusion and premixed flames were performed (Bui-Pham 1992, Ilincic 1995) and it was found that $CH_4/NO_2/O_2$ diffusion flame structures were quiet different from those of hydrocarbon flames. For CH_4/NO_2 diffusion flames, fuel and oxidizer were consumed in two separated layers. No solution for pure CH_4/NO_2 premixed flames could be obtained (Bui-Pham 1992).

In the present work, premixed $CH_4/NO_2/O_2$ and $CH_2O/NO_2/O_2$ flame systems are investigated numerically with full chemical-kinetic mechanisms and reduced chemical-kinetic mechanisms. Two different definitions of equivalence ratio were introduced to study the influences of NO_2 on the burning velocities. The flame structures under various conditions are studied and the influence of NO_2 on the structure of the flame was explored.

3.2 Governing Equations and Formulations

The configuration considered here for premixed flames is a planar, steady state, one-dimensional, laminar flow. The flow direction is denoted by x and the flow Mach-number is small. The initial unburned reactants comes from $x = -\infty$ and the products are located at $x = \infty$. There are no heat losses from the flame.

Since we assume that the flow Mach-number is small, so for this kind flow, the momentum equation degenerates to pressure to be constant in the whole flow field. The governing equations of mass, species, and energy are

$$\left.\begin{array}{rrcl} \text{Mass :} & \dot{M} & = & \rho u = \text{constant}, \\ \text{Species :} & \dot{M}\frac{dY_i}{dx} & = & -\frac{d}{dx}(\rho Y_i V_i) + \dot{m}_i, \quad i = 1,\ 2,\ ...,\ K, \\ \text{Energy :} & \dot{M}c_p\frac{dT}{dx} & = & \frac{d}{dx}(\lambda\frac{dT}{dx}) - \sum_{i=1}^{n} h_i\dot{m}_i - \sum_{i=1}^{n} c_{pi}\rho Y_i V_i\frac{dT}{dx}. \end{array}\right\} \tag{3.1}$$

The system is closed by the ideal gas law

$$\rho = p\hat{W}/RT. \tag{3.2}$$

In the equations, x denotes the spatial coordinate fixed to the flame. ρ is the density; u the flow velocity; $\dot{M}$ the mass flow rate per unit area. Y_i and V_i are the mass fraction and dif-

fusion velocity of species i respectively. $\dot{m}_i$ denotes the mass production rate per unit volume of species i; c_p the constant pressure heat capacity of ith species; T the temperature; λ the heat conductivity of the mixture; h_i the specific enthalpy of species i; $\hat{W}$ the mean molecular weight of the mixture; p the pressure; and R is the universal gas constant.

Boundary conditions are: at $x \to -\infty$, $T = T_{-\infty}$, $Y_i = Y_{i,-\infty}$, and all gradients vanish both at $x \to -\infty$ and $x \to \infty$.

The infinite domain shown here is difficult to be used in practical numerical calculations. So it is truncated to a finite size of L. The new domain is from $x = 0$ to $x = L$. An ignition temperature T_i is introduced at $x = 0$. Below this temperature, the reactions are frozen. Thus the boundary conditions used in practical numerical calculations are the following

at $x = 0$

$$\left.\begin{aligned} T &= T_i, \\ \left(Y_i + \frac{\rho Y_i V_i}{M}\right)_{x=0} &= Y_{i,-\infty}, \\ \left(T - \frac{\lambda}{c_p M}\frac{dT}{dx}\right)_{x=0} &= T_{-\infty}, \end{aligned}\right\} \tag{3.3}$$

at $x = L$

$$\left.\begin{aligned} \left(\frac{dT}{dx}\right)_{x=L} &= 0, \\ \left(\frac{dY_i}{dx}\right)_{x=L} &= 0. \end{aligned}\right\} \tag{3.4}$$

One extra boundary condition shown here is used to get the flow rate $\dot{M}$. For $CH_4/NO_2/O_2$ premixed flames, the following conditions are given

$$\left.\begin{aligned} T &= T_{-\infty} = 298\ K, \\ X_{CH_4} &= X_{CH_4,-\infty}, \quad X_{NO_2} = X_{NO_2,-\infty}, \quad X_{O_2} = X_{O_2,-\infty}, \\ X_{i,-\infty} &= 0, \quad i \neq CH_4,\ NO_2,\ O_2, \end{aligned}\right\} \tag{3.5}$$

and for $CH_2O/NO_2/O_2$ flames,

$$\left.\begin{aligned} T &= T_{-\infty} = 423\ K, \\ X_{CH_4} &= X_{CH_4,-\infty}, \quad X_{NO_2} = X_{NO_2,-\infty}, \quad X_{O_2} = X_{O_2,-\infty}, \\ X_{i,-\infty} &= 0, \quad i \neq CH_4,\ NO_2,\ O_2. \end{aligned}\right\} \tag{3.6}$$

In Eqs. 3.5 and 3.6, X_i represents the molar fraction of species i. For $CH_2O/NO_2/O_2$ systems, $T_{-\infty} = 423$ K instead of 298 K was chosen to be the initial temperature. Since in experiments, CH_2O can not be stored as gas in a cylinder because of its reactivity, particularly with itself to form solid polymer, so a gaseous CH_2O generator at certain temperature (say 423 K) is needed to supply a continuous stream of gaseous CH_2O (Branch et al. 1991).

In order to define the equivalence ratio ϕ, we assume that one-step reactions occur according to

$$\left.\begin{array}{l} CH_4 + NO_2 + O_2 \rightarrow CO_2 + N_2 + 2H_2O, \\ CH_2O + \frac{1}{2}(NO_2 + O_2) \rightarrow CO_2 + \frac{1}{4}N_2 + H_2O. \end{array}\right\} \tag{3.7}$$

The equivalence ratio is defined as

$$\phi = \frac{[Y_F/Y_O]}{[Y_F/Y_O]_{st}}, \tag{3.8}$$

here Y_i is the mass fraction of species i, the subscripts F and O represent fuel and oxidizer respectively, and the subscript st represents the stoichiometric condition.

As they were used before (Bui-Pham 1992), two different systems are defined here: 1) CH_4 for $CH_4/NO_2/O_2$ flames or CH_2O for $CH_2O/NO_2/O_2$ flames as the fuel, and NO_2+O_2 as the oxidizer. The ratio of the initial molar fractions of NO_2 and O_2 is kept to be unity. 2) CH_4 + NO_2 for $CH_4/NO_2/O_2$ flames or, CH_2O+$\frac{1}{2}NO_2$ for $CH_2O/NO_2/O_2$ flames, as the fuel, and O_2 as the oxidizer. In the second definition, the ratio of the initial molar fractions of CH_4 and NO_2 is kept as unity for $CH_4/NO_2/O_2$ flames, and the ratio of the initial molar fractions of CH_2O and NO_2 is kept as two for $CH_2O/NO_2/O_2$ flames.

The chemical-kinetic mechanism of $CH_4/NO_2/O_2$ flame systems is shown in Table 3.1. This mechanism was used before in (Bui-Pham 1992) for both premixed and diffusion $CH_4/NO_2/O_2$ flames. Table 3.2 shows the chemical-kinetic mechanism of $CH_2O/NO_2/O_2$ flame systems.

3.3 Results and Discussions

3.3.1 $CH_4/NO_2/O_2$ Flames

The calculations were done for the initial temperatures as specified in the previous section and at pressure being one atmosphere. Figure 3.1 shows the flame temperature as a function of equivalence ratio. For the system corresponding to the first definition of ϕ, the flame temperature first increases with the increasing value of ϕ and attains a maximum at $\phi = 1.1$, then it decreases quickly with the increasing value of ϕ. For the system corresponding to the second definition of ϕ, after the flame temperature attains a maximum value, it then decreases gradually and finally approaches a constant value. This is because that as ϕ increases, the oxidizer, O_2, decreases and the fuel CH_4 + NO_2 goes to a constant composition. As $\phi \rightarrow \infty$, O_2 vanishes, and the fuel goes to CH_4 + NO_2 which itself contains an oxidizer NO_2.

Table 3.1: Chemical-Kinetic Mechanism of $CH_4/NO_2/O_2$ Flames

NO.	Reaction[a]	A_i	n_i	E_i
1	$CH_4 + H = CH_3 + H_2$	2.20E04	3.0	8750.0
2	$CH_4 + OH = CH_3 + H_2O$	1.60E06	2.1	2460.0
3	$CH_4 + O = CH_3 + OH$	1.60E06	2.36	7400.0
4	$CH_3 + H + M = CH_4 + M$	1.90E36	-7.0	9050.0
5	$CH_3 + O = CH_2O + H$	6.80E13	0.0	0.0
6	$CH_3 + O_2 = CH_3O + O$	7.00E13	0.0	25652.0
7	$CH_3 + O_2 = CH_2O + OH$	7.00E13	0.0	25652.0
8	$CH_2O + H = HCO + H_2$	2.51E13	0.0	3991.0
9	$CH_2O + OH = HCO + H_2O$	3.00E13	0.0	1195.0
10	$CH_3O + M = CH_2O + H + M$	2.40E13	0.0	28812.0
11	$CH_3O + H = CH_3 + OH$	1.00E14	0.0	0.0
12	$CH_3O + H = CH_2O + H_2$	2.00E13	0.0	0.0
13	$CH_3O + O_2 = CH_2O + HO_2$	6.30E10	0.0	2600.0
14	$HCO + M = H + CO + M$	1.60E14	0.0	14700.0
15	$HCO + H = CO + H_2$	4.00E13	0.0	0.0
16	$CO + OH = CO_2 + H$	1.51E07	1.3	-758.0
17	$H + O_2 = OH + O$	2.00E14	0.0	16800.0
18	$H_2 + O = OH + H$	1.80E10	1.0	8826.0
19	$OH + H_2 = H_2O + H$	1.17E09	1.3	3626.0
20	$OH + OH = H_2O + O$	6.00E08	1.3	0.0
21	$H + O_2 + M^b = HO_2 + M$	2.30E18	-0.8	0.0
22	$H + OH + M^b = H_2O + M$	2.20E22	-2.0	0.0
23	$H + H + M^b = H_2 + M$	1.80E18	-1.0	0.0
24	$OH + HO_2 = H_2O + O_2$	2.00E13	0.0	1000.0
25	$H + HO_2 = 2OH$	1.50E14	0.0	1004.0
26	$H + HO_2 = H_2 + O_2$	2.50E13	0.0	700.0
27	$HO_2 + HO_2 = H_2O_2 + O_2$	2.00E12	0.0	0.0
28	$H_2O_2 + M = OH + OH + M$	1.30E17	0.0	45500.0
29	$H_2O_2 + H = HO_2 + H_2$	1.60E12	0.0	3800.0
30	$H_2O_2 + OH = H_2O + HO_2$	1.00E13	0.0	1800.0
31	$NO_2 + N = 2NO$	4.00E12	0.0	0.0
32	$NO_2 + N = N_2 + O_2$	1.00E12	0.0	0.0
33	$N + HO_2 = NO + OH$	1.00E13	0.0	2000.0
34	$NO_2 + M = NO + O + M$	1.10E16	0.0	65570.0

(to be continued on next page)

Table 3.1 (continued)

NO.	Reaction	A_i	n_i	E_i
35	$2NO_2 = 2NO + O_2$	2.00E12	0.0	26620.0
36	$NO + M = N + O + M$	4.00E20	-1.5	150000.0
37	$2NO = N_2 + O_2$	1.30E14	0.0	75630.0
38	$NO_2 + CH_3 = CH_3O + NO$	1.50E13	0.0	0.0
39	$NO_2 + H = NO + OH$	3.50E14	0.0	1500.0
40	$N + NO = N_2 + O$	3.27E12	0.3	0.0
41	$N + O_2 = NO + O$	6.40E09	1.0	6280.0
42	$NO + H = N + OH$	2.63E14	0.0	50410.0
43	$NO_2 + O = NO + O_2$	1.00E13	0.0	600.0
44	$NO_2 + HCO = CO_2 + H + NO$	1.50E12	0.0	-430.0
45	$NO_2 + CO = CO_2 + NO$	1.26E14	0.0	27600.0

[a] Rate constants are in the form $k_i = A_i T^{n_i} \exp[-E_i/(RT)]$. Units are moles, cubic centimeters, seconds, Kelvins and cal/mole.

[b] Third-body efficiencies are H_2O: 6.5, CO_2: 1.5, CO: 0.75, O_2: 0.4, N_2: 0.4, all other species 1.0.

Table 3.2: Chemical-Kinetic Mechanism of $CH_2O/NO_2/O_2$ Flames

NO.	Reaction[a]	A_i	n_i	E_i
1	$CH_2O + OH = HCO + H_2O$	3.00E13	0.0	1195.0
2	$CH_2O + H = HCO + H_2$	2.51E13	0.0	3991.0
3	$CH_2O + O_2 = HCO + HO_2$	2.00E13	0.0	38950.0
4	$CH_2O + HO_2 = HCO + H_2O_2$	2.00E12	0.0	11660.0
5	$CH_2O + M = HCO + H + M$	3.31E16	0.0	81000.0
6	$CH_2O + O = HCO + OH$	1.80E13	0.0	3080.0
7	$HCO + M = H + CO + M$	1.60E14	0.0	14700.0
8	$HCO + H = CO + H_2$	4.00E13	0.0	0.0
9	$CO + OH = CO_2 + H$	1.51E07	1.3	-758.0
10	$H + O_2 = OH + O$	2.00E14	0.0	16800.0
11	$H_2 + O = OH + H$	1.80E10	1.0	8826.0
12	$OH + H_2 = H_2O + H$	1.17E09	1.3	3626.0
13	$OH + OH = H_2O + O$	6.00E08	1.3	0.0
14	$H + H + M^b = H_2 + M$	1.80E18	-1.0	0.0
15	$H + OH + M^b = H_2O + M$	2.20E22	-2.0	0.0
16	$H + O_2 + M^b = HO_2 + M$	2.30E18	-0.8	0.0
17	$H + HO_2 = 2OH$	1.50E14	0.0	1004.0
18	$H + HO_2 = H_2 + O_2$	2.50E13	0.0	700.0
19	$OH + HO_2 = H_2O + O_2$	2.00E13	0.0	1000.0
20	$HO_2 + HO_2 = H_2O_2 + O_2$	2.00E12	0.0	0.0
21	$H_2O_2 + M = OH + OH + M$	1.30E17	0.0	45500.0
22	$H_2O_2 + H = HO_2 + H_2$	1.60E12	0.0	3800.0
23	$H_2O_2 + OH = H_2O + HO_2$	1.00E13	0.0	1800.0
24	$NO_2 + H = NO + OH$	3.47E14	0.0	1470.0
25	$NO + H = N + OH$	2.63E14	0.0	50410.0
26	$NO_2 + O = NO + O_2$	1.00E13	0.0	600.0
27	$NO_2 + N = 2NO$	4.00E12	0.0	0.0
28	$NO_2 + N = N_2 + O_2$	1.00E12	0.0	0.0
29	$NO_2 + M = NO + O + M$	1.10E16	0.0	65570.0
30	$2NO_2 = 2NO + O_2$	2.00E12	0.0	26620.0
31	$NO_2 + HCO = CO_2 + H + NO$	1.50E12	0.0	-430.0
32	$NO_2 + CO = CO_2 + NO$	1.26E14	0.0	27600.0
33	$CO_2 + N = NO + CO$	1.90E11	0.0	3400.0
34	$N + HO_2 = NO + OH$	1.00E13	0.0	2000.0

(to be continued on next page)

Table 3.2 (continued)

NO.	Reaction	A_i	n_i	E_i
35	$NO + M = N + O + M$	4.00E20	-1.5	150000.0
36	$2NO = N_2 + O_2$	1.30E14	0.0	75630.0
37	$N + NO = N_2 + O$	3.27E12	0.3	0.0
38	$N + O_2 = NO + O$	6.40E09	1.0	6280.0
39	$CH_2O + NO_2 = HCO + HONO$	2.94E11	0.0	12850.0
40	$HCO + NO_2 = CO + HONO$	1.24E23	-3.29	2355.0
41	$HCO + NO = CO + HNO$	7.20E13	-0.40	0.0
42	$CH_2O + O = CO_2 + 2H$	3.50E05	2.40	1360.0
43	$HCO + OH = H_2O + CO$	3.00E13	0.00	0.0
44	$OH + NO + M^b = HONO + M$	1.60E14	-0.50	0.0
45	$HNO + OH = H_2O + NO$	1.30E12	0.50	1990.0
46	$CH_2O + M = H_2 + CO$	2.30E15	0.50	64800.0
47	$H + NO + M^b = HNO + M$	5.40E15	0.00	-600.0
48	$HONO + OH = H_2O + NO_2$	1.00E13	0.00	3300.0
49	$HNO + H = H_2 + NO$	1.30E13	0.00	3970.0
50	$HNO + O = OH + NO$	5.00E11	0.50	1990.0
51	$HCO + O = H + CO_2$	3.00E13	0.00	0.0
52	$HCO + O = OH + CO$	3.00E13	0.00	0.0
53	$O + O + M^b = O_2 + M$	1.89E13	0.00	-1788.0
54	$CO + O + M^b = CO_2 + M$	6.17E14	0.00	3000.0
55	$CO + O_2 = CO_2 + O$	1.60E13	0.00	41000.0
56	$HNO + O = NO_2 + H$	5.00E10	0.50	2000.0
57	$HCO + HNO = CH_2O + NO$	2.00E12	0.00	5000.0
58	$H + HONO = H_2 + NO_2$	1.00E12	0.00	1000.0

[a] Rate constants are in the form $k_i = A_i T^{n_i} \exp[-E_i/(RT)]$. Units are moles, cubic centimeters, seconds, Kelvins and cal/mole.

[b] Third-body efficiencies are H_2O: 6.5, CO_2: 1.5, CO: 0.75, O_2: 0.4, N_2: 0.4, all other species 1.0.

[b] Third-body efficiencies are H_2O : 6.5, CO_2 : 1.5, CO : 0.75, O_2 : 0.4, N_2 : 0.4, all other species 1.0.

Figure 3.2 gives the plots of burning velocities, v_u, as functions of equivalence ratio ϕ. For the system corresponding to the first definition of ϕ, as ϕ increases, the burning velocity increases, then attains a maximum value around $\phi = 0.9$. As ϕ increases further, the burning velocity drops quickly. This behavior is similar to that of a usual two reactants (fuel and oxidizer) premixed flame system. While for the system corresponding to the second definition

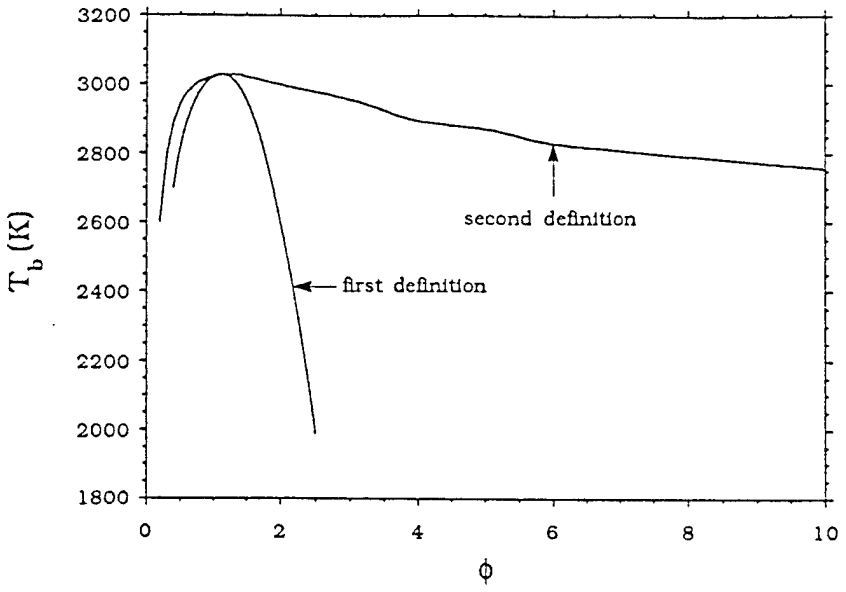

Figure 3.1: Variation of flame temperature as a function of equivalence ratio for $CH_4/NO_2/O_2$ flame system

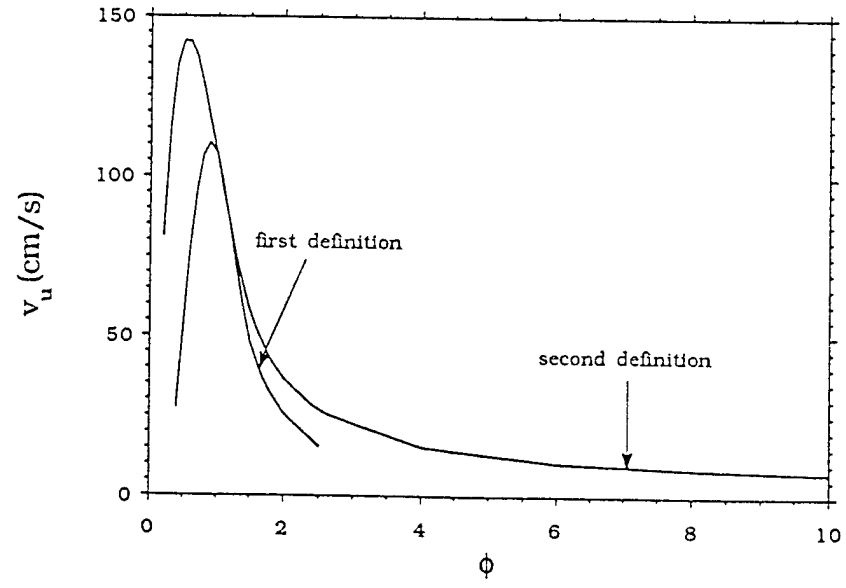

Figure 3.2: Variation of burning velocity as a function of equivalence ratio for $CH_4/NO_2/O_2$ flame system

of ϕ, there are some interesting different phenomena. As ϕ increases, the burning velocity increases, then attains a maximum value around $\phi = 0.5$. As ϕ increases further, the burning velocity decreases gradually to a constant value which is 3.3 cm/s corresponding to $\phi = \infty$. These facts suggest that NO_2 behaviors like an inhibitor and, a pure CH_4+NO_2 premixed flame is a very weak flame. The reasons will be explored later in the discussions of the flame structures.

The structures for $CH_4/NO_2/O_2$ flames with the second definition of equivalence ratio are shown in Figures 3.3 - 3.14. The corresponding equivalence ratios are 0.3, 0.5, 0.9 and ∞. $\phi = 0.3$ represents the region in which the burning velocity increases with the increasing values of ϕ, $\phi = 0.5$ corresponds to the maximum burning velocity, $\phi = 0.9$ represents the region where burning velocity decreases with the increasing values of ϕ. At $\phi = 0.9$ the burning velocity is roughly the same as that at $\phi = 0.3$. $\phi = \infty$ means that there is no O_2 presenting in the system, the reactants are CH_4 and NO_2 with an initial composition, $X_{CH_4,-\infty} : X_{O_2,-\infty} = 1 : 1$.

For $\phi = 0.3$ and 0.5, as it shows in Figures 3.3 and 3.6, the concentration of oxygen decreases to a constant value. For ϕ =0.9, as seen in Figure 3.9, the concentration of oxygen decreases first to a minimum value and then increases gradually. The decreasing trend of oxygen concentration can be attributed to the reactions of O_2 with the radicals. This trend will soon be balanced or even suppressed (in the case $\phi = 0.9$) by the oxygen production reaction

$$2NO = N_2 + O_2.$$

It can be seen from Figures 3.3, 3.6 and 3.9 that NO_2 and CH_4 are consumed almost in the same region, and NO_2 disappears earlier than CH_4. The trend of NO_2 profile shown here is in consistent with those of experimental measurements and numerical simulations in (Zabarnick 1991), but in disagreement with the experimental results in (Sadeqi 1987, Zabarnick 1991) in which only partial consumption of NO_2 in the flames was observed. This, as discussed in (Zabarnick 1991), is likely due to the use of a quartz microprobe and gas chromatography analysis. It is possible that NO_2 could be formed in the probing and analysis processes due to the reaction

$$2NO + O_2 \rightarrow 2NO_2.$$

The almost simultaneous disappearances of NO_2 and CH_4 make premixed $CH_4/NO_2/O_2$ flames very different from $CH_4/NO_2/O_2$ diffusion flames. For the diffusion flames, as it was observed in (Bui-Pham 1992, Ilincic 1995), the consumptions of CH_4 and NO_2 occur in two different regions.

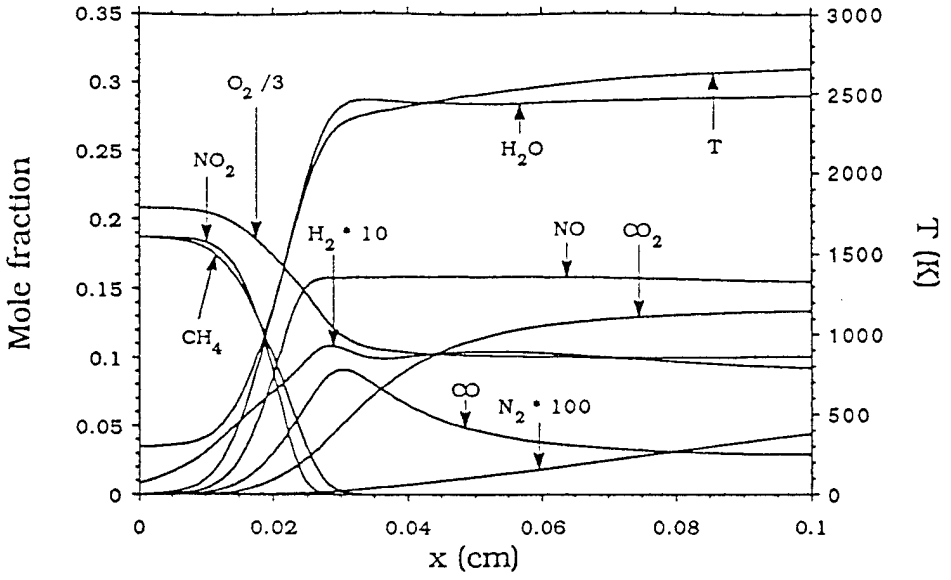

Figure 3.3: Stable species profiles at $\phi = 0.3$ for $CH_4/NO_2/O_2$ flame system with the second definition of equivalence ratio

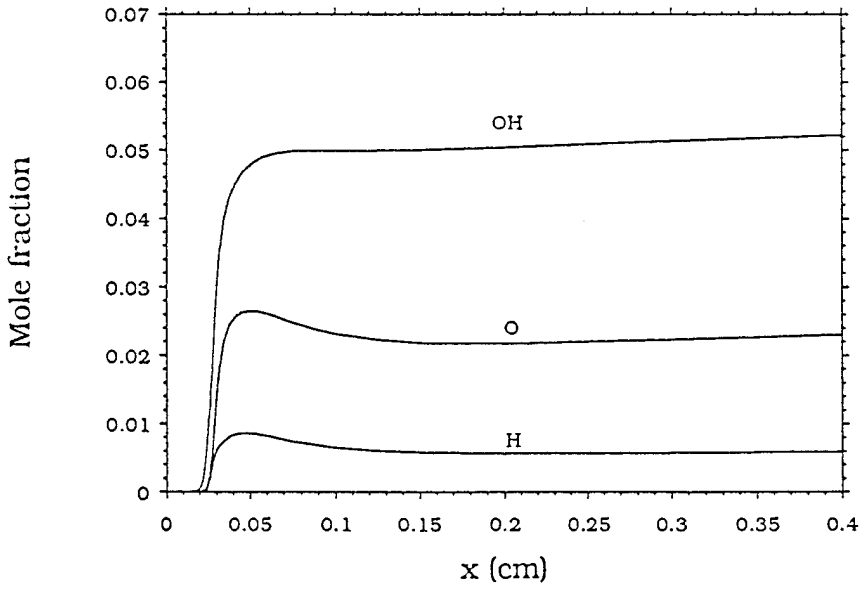

Figure 3.4: Radical species profiles at $\phi = 0.3$ for $CH_4/NO_2/O_2$ flame system with the second definition of equivalence ratio

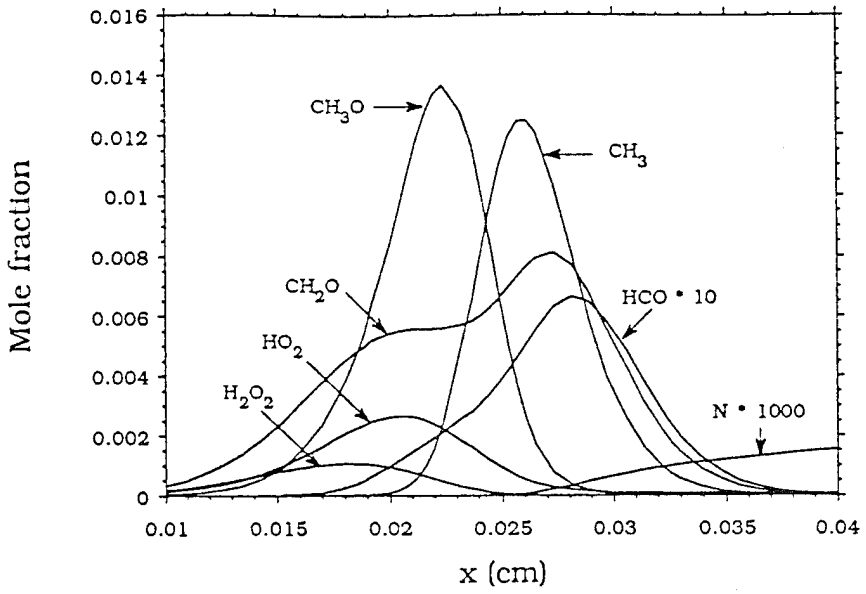

Figure 3.5: Intermediate species profiles at $\phi = 0.3$ for $CH_4/NO_2/O_2$ flame system with the second definition of equivalence ratio

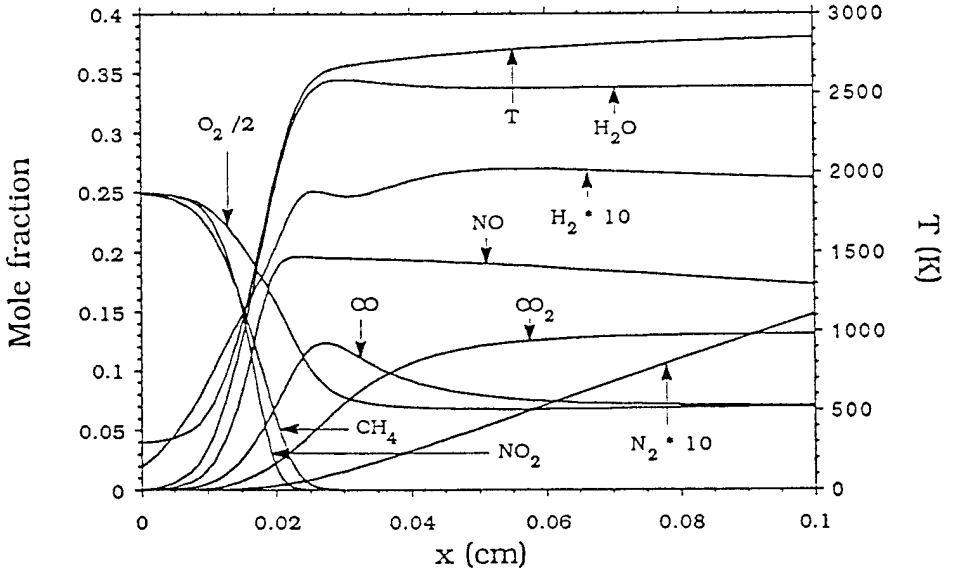

Figure 3.6: Stable species profiles at $\phi = 0.5$ for $CH_4/NO_2/O_2$ flame system with the second definition of equivalence ratio

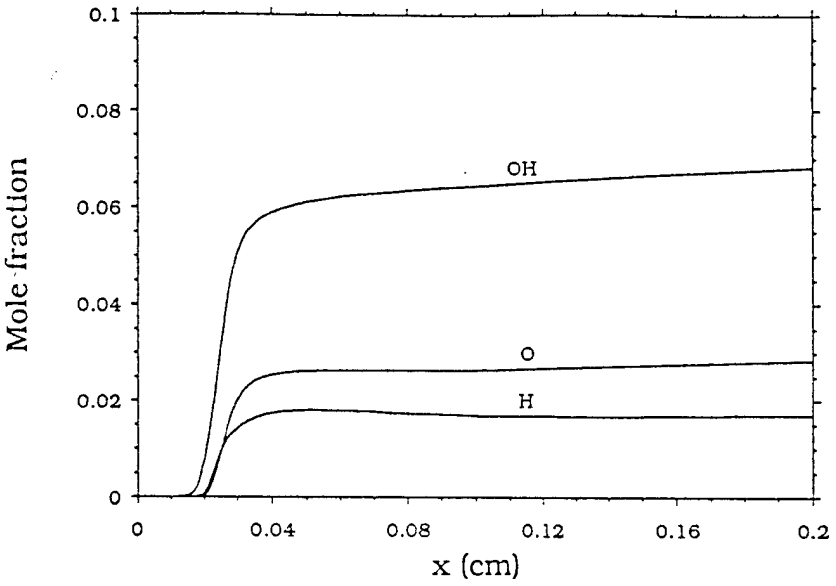

Figure 3.7: Radical species profiles at $\phi = 0.5$ for $CH_4/NO_2/O_2$ flame system with the second definition of equivalence ratio

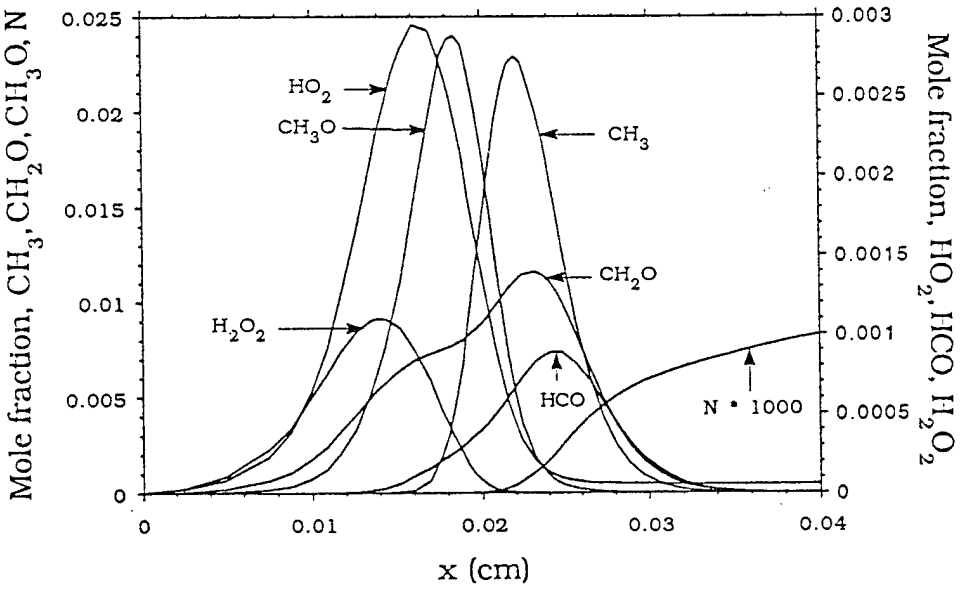

Figure 3.8: Intermediate species profiles at $\phi = 0.5$ for $CH_4/NO_2/O_2$ flame system with the second definition of equivalence ratio

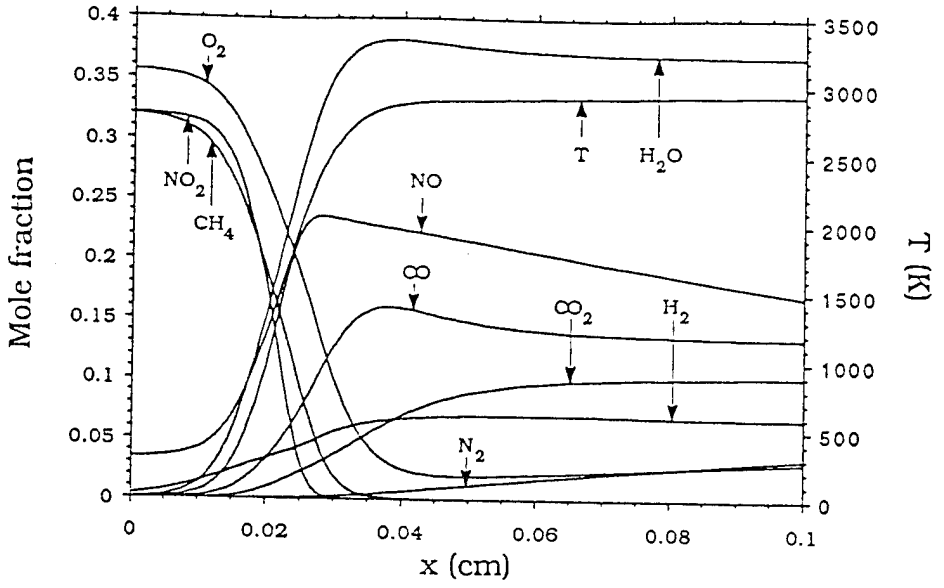

Figure 3.9: Stable species profiles at $\phi = 0.9$ for $CH_4/NO_2/O_2$ flame system with the second definition of equivalence ratio

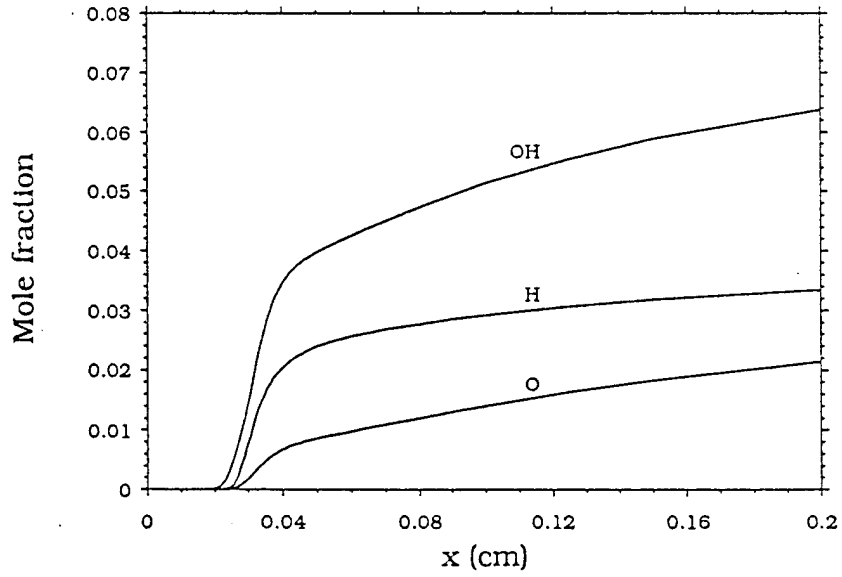

Figure 3.10: Radical species profiles at $\phi = 0.9$ for $CH_4/NO_2/O_2$ flame system with the second definition of equivalence ratio

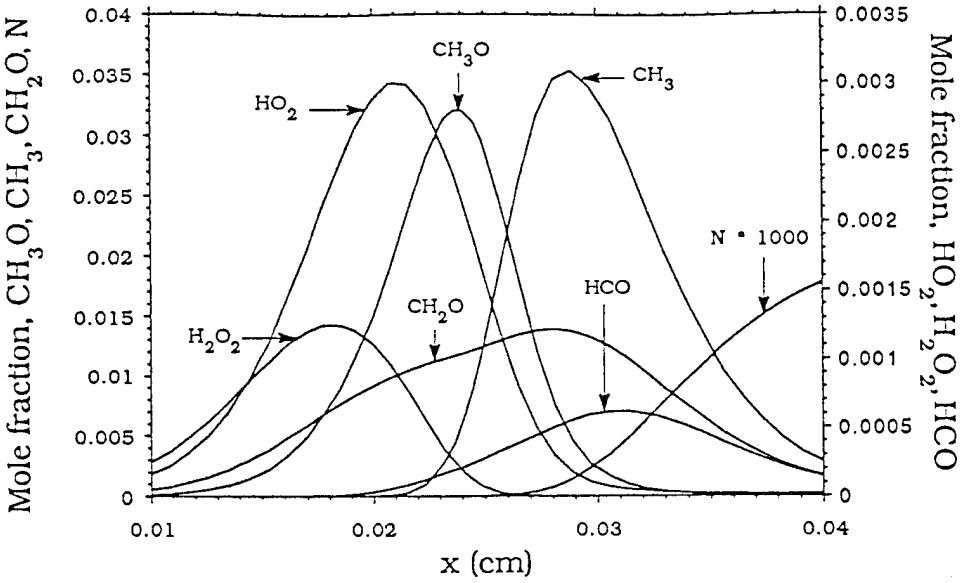

Figure 3.11: Intermediate species profiles at $\phi = 0.9$ for $CH_4/NO_2/O_2$ flame system with the second definition of equivalence ratio

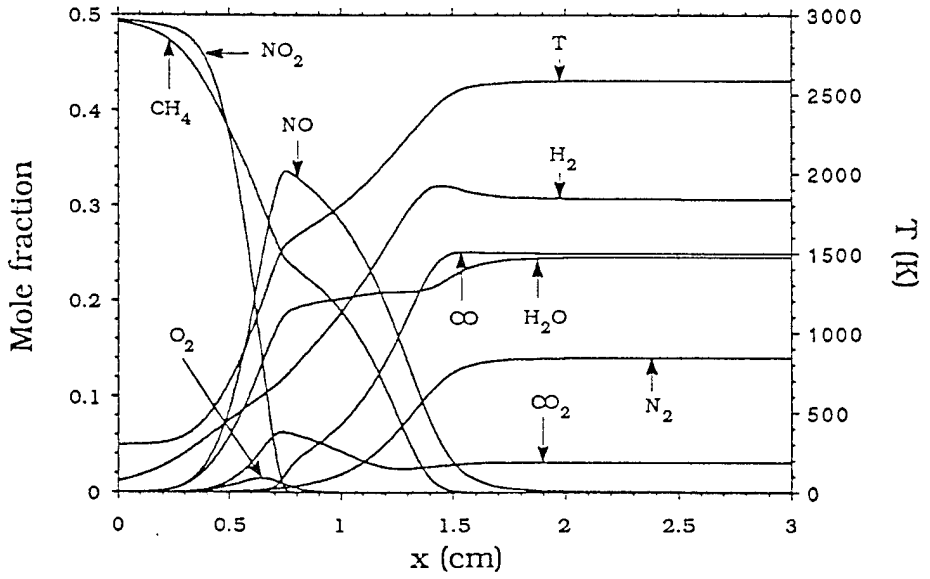

Figure 3.12: Stable species profiles at $\phi \to \infty$ for $CH_4/NO_2/O_2$ flame system with the second definition of equivalence ratio

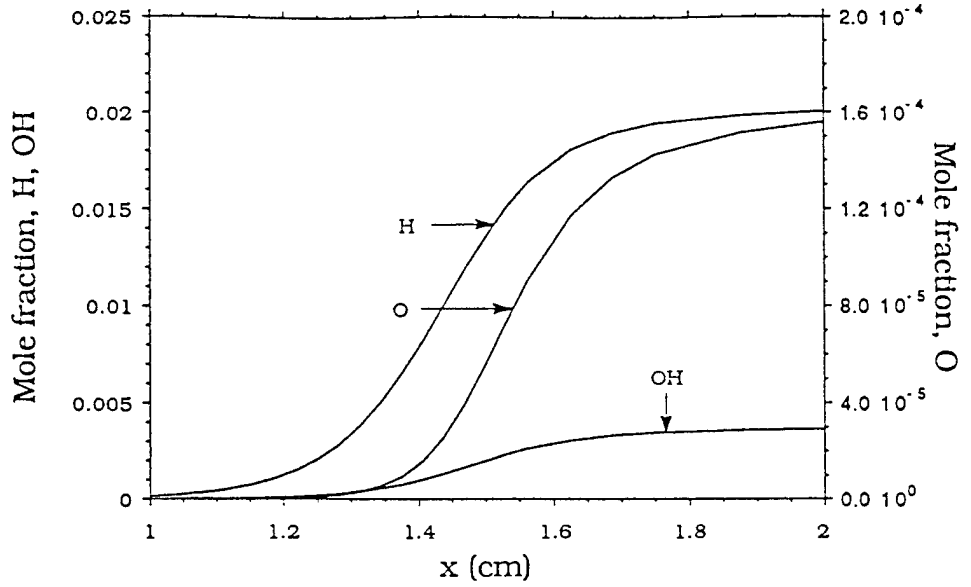

Figure 3.13: Radical species profiles at $\phi \rightarrow \infty$ for $CH_4/NO_2/O_2$ flame system with the second definition of equivalence ratio

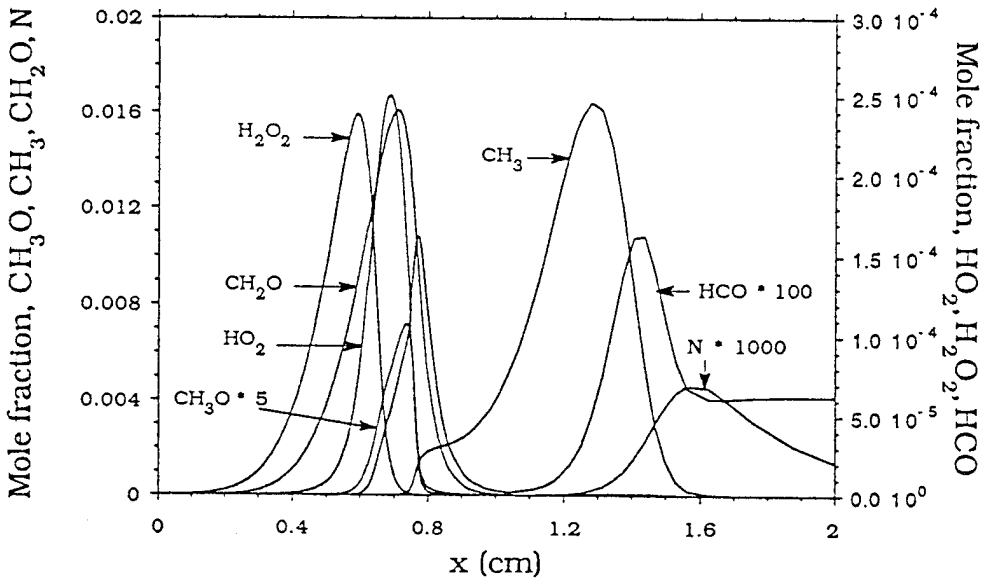

Figure 3.14: Intermediate species profiles at $\phi \rightarrow \infty$ for $CH_4/NO_2/O_2$ flame system with the second definition of equivalence ratio

Maximum values of H_2O, NO, H_2, and CO occur near the region where CH_4 and NO_2 disappear. They are produced from the consumptions of CH_4, O_2 and the decomposition of NO_2. This is similar to methane-air premixed flames where a fuel consumption layer exists to form H_2, CO and H_2O. After the formation of CO, NO, and H_2, NO is further attacked by the radicals to form N_2, CO is oxidized to form CO_2, and H_2 is oxidized to form H_2O. This layer is similar to the oxidation layer of H_2 and CO of methane-air flames (Seshadri & Peters 1988b, Seshadri & Göttgens 1991, Seshadri & Peters 1988a, Treviño & Williams 1988).

The profiles of OH, O, and H in Figures 3.4, 3.7 and 3.10 show that these radicals always disappear at the same point where NO_2 disappears. This suggests that NO_2 is a radical destroyer and, indeed it is a stronger radical destroyer than CH_4. In the combustion process, NO_2 competes with CH_4 for radicals. Since CH_4/NO_2 premixed flames are very weak flames, this competition makes NO_2 act like a fuel and decreases the levels of radical concentrations, and makes the flame difficult to propagate. Hence, the presence of oxygen in the flame is necessary to maintain a certain level of radical concentration and keep the flame propagating. This conclusion is supported by the calculations of pure CH_4 + NO_2 combustion which are shown in Figures 3.12 - 3.14. The maximum values of the molar fractions of the radicals H, OH, and O for the the pure CH_4 + NO_2 flame are of orders of 10^{-2}, 10^{-3} and 10^{-4}, while those for $CH_4/NO_2/O_2$ flames with $\phi = 0.3$, 0.5, and 0.9 are of orders of 10^{-2}. The absence of oxygen decreases the levels of radical concentrations and thus makes the flame harder to propagate than the flame with initial oxygen does. The flame velocity for the pure CH_4 + NO_2 flame is 3.3 cm/s, while for the flames with $\phi = 0.3$, 0.5 and 0.9, the flame velocities are 116.1, 142.1 and 117.9 cm/s respectively. They are much larger than 3.3 cm/s. A pure CH_4 + NO_2 flame is a very weak flame. This explains the difficulties encountered by Bui-Pham (1992) in getting a pure methane, pure nitrogen dioxide flame, and the difficulties met by Zabarnick (1991) in calculating a freely propagating flame with high starting concentrations of NO_2 and, why Branch et al. (1991) could not stabilize flames in rich mixtures of $CH_4/NO_2/O_2$ and stable flames in lean mixture could only be obtained with difficulty.

The profiles of intermediate species CH_3, CH_3O, CH_2O, HCO, HO_2, and H_2O_2 are plotted in Figures 3.5, 3.8, 3.11 and 3.13.

The structures of the $CH_4/NO_2/O_2$ flames with the first definition of equivalence ratio ϕ are essentially the same as those discussed above.

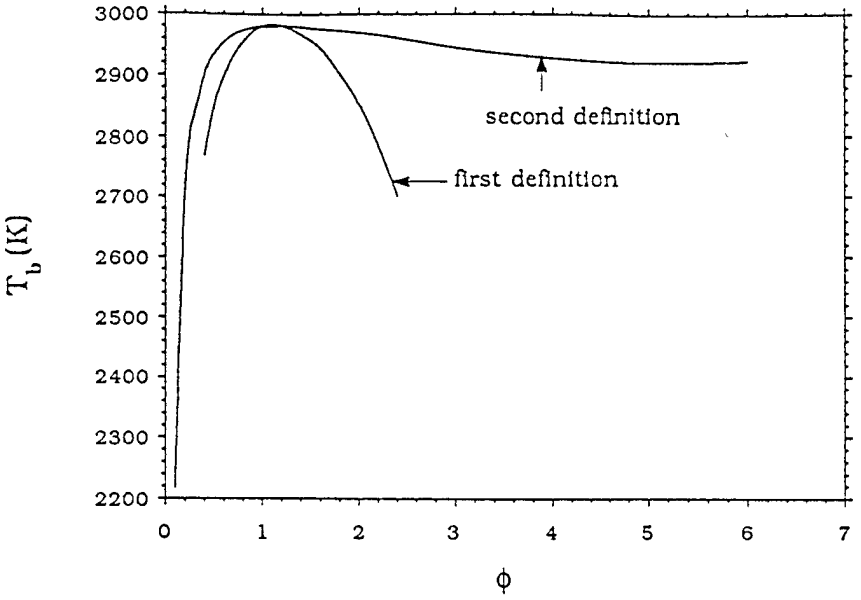

Figure 3.15: Variation of flame temperature as a function of equivalence ratio for $CH_2O/NO_2/O_2$ flame system

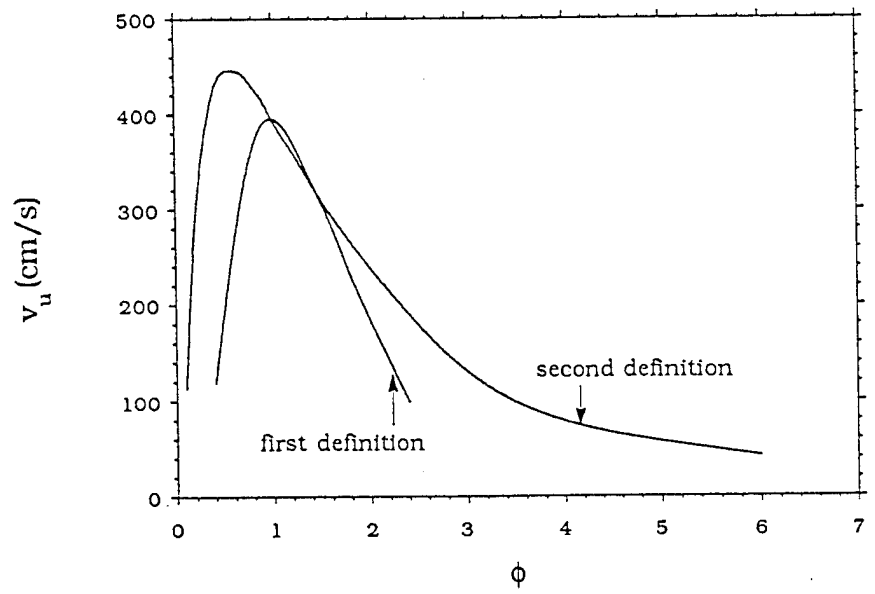

Figure 3.16: Variation of burning velocity as a function of equivalence ratio for $CH_2O/NO_2/O_2$ flame system

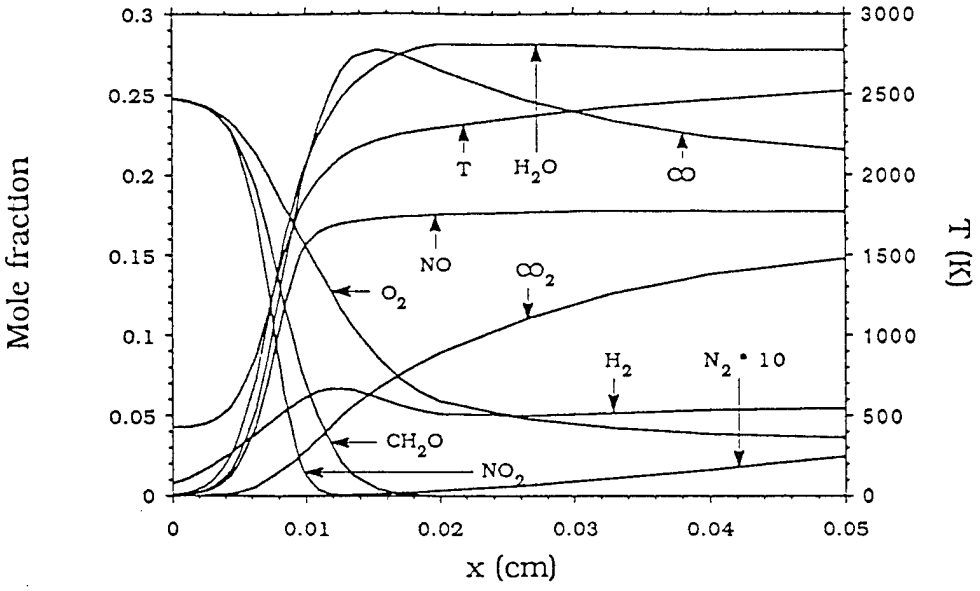

Figure 3.17: Stable species profiles at $\phi = 1$ for $CH_2O/NO_2/O_2$ flame system with the second definition of equivalence ratio

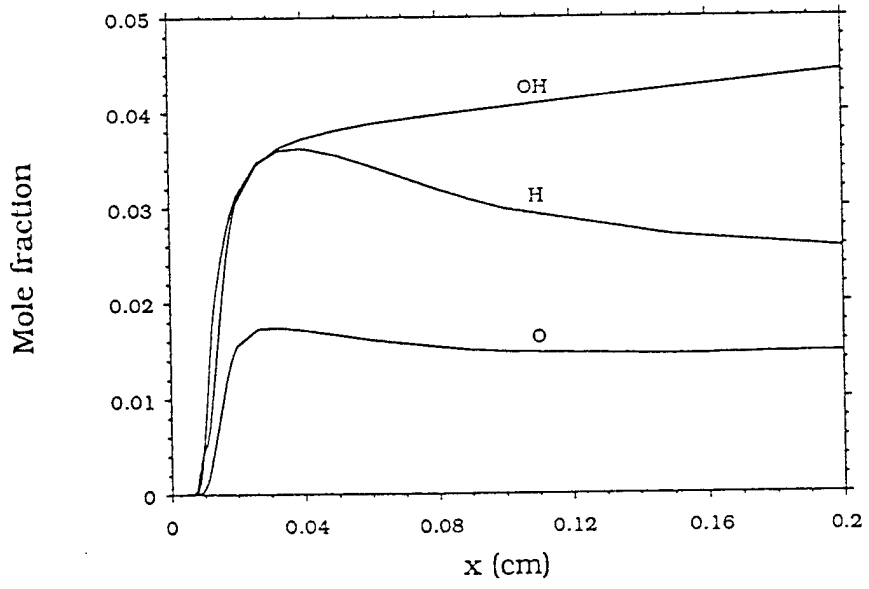

Figure 3.18: Radical species profiles at $\phi = 1$ for $CH_2O/NO_2/O_2$ flame system with the second definition of equivalence ratio

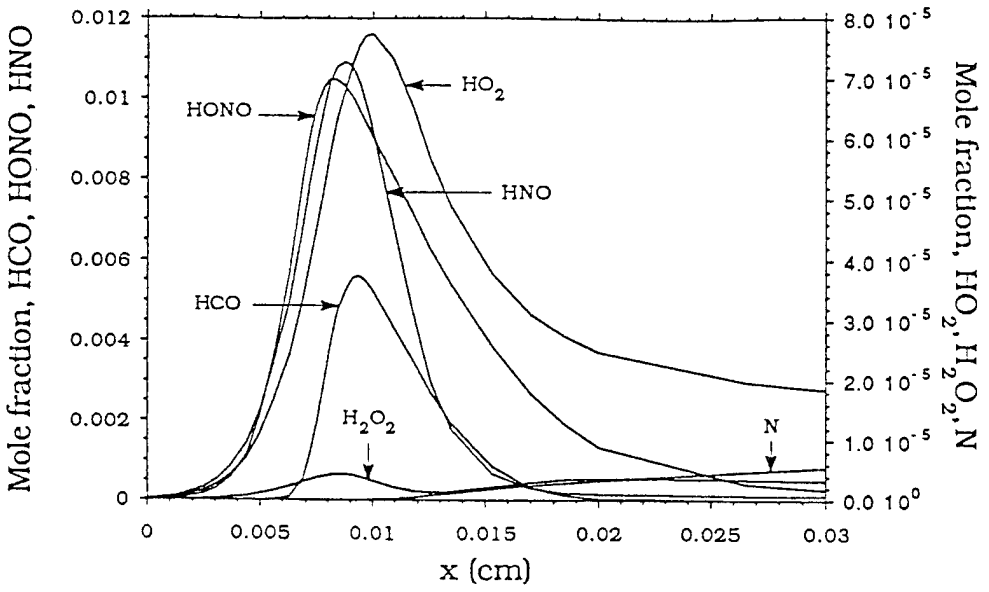

Figure 3.19: Intermediate species profiles at $\phi = 1$ for $CH_2O/NO_2/O_2$ flame system with the second definition of equivalence ratio

3.3.2 $CH_2O/NO_2/O_2$ Flames

Figures 3.15 and 3.16 show the temperature and burning velocity as functions of equivalence ratio for $CH_2O/NO_2/O_2$ systems. They are very similar to the temperature and burning velocity profiles shown in Figures 3.1 and 3.2 for $CH_4/NO_2/O_2$ systems. The maximum value of burning velocity of $CH_2O/NO_2/O_2$ systems is 446 cm/s at ϕ= 0.6 with the second definition of equivalence ratio, and is 395.4 cm/s at ϕ =1.0 with the first definition of equivalence ratio. For the pure CH_2O + NO_2 flame with an initial composition, $X_{CH_2O} : X_{NO_2}$ = 2:1, which corresponds to $\phi = \infty$, the burning velocity is 35.7 cm/s. Although this is small compared with the maximum value of 446 cm/s, but it is close to the burning velocity of a methane-air premixed flame near stoichiometry. So we can still expect a stable flame for pure CH_2O + NO_2 systems, as it was observed in (Branch et al. 1991).

Only the structures corresponding to the flame with equivalence ϕ = 1.0 were plotted. The profiles are shown in Figures 3.17 - 3.19. They actually are similar to the structures of $CH_4/NO_2/O_2$ flames. Indeed the similarities in flame structures result in the similarities in the behaviors of burning velocity with equivalence ratio.

3.4 The Reduced Mechanism for Premixed $CH_4/NO_2/O_2$ Flames

In the previous sections, the structures of premixed $CH_4/NO_2/O_2$ and $CH_2O/NO_2/O_2$ flames were studied using full chemical-kinetic mechanisms. In this section and the following section, the structures of these flames will be studied by using reduced mechanisms. As it was done before, a reduced mechanism is achieved from a full mechanism by introducing steady-state assumptions for some species. Here for $CH_4/NO_2/O_2$ premixed flames, the full mechanism is the one shown in Table 3.1. Steady-state assumptions are made for H_2O_2, HCO, HO_2, CH_3O, CH_2O, CH_3, O, and N species. In numerical calculations, a steady-state assumption for a species is effected by putting the diffusion and convection terms of this species to zero. Since no convergence was achieved for flames with steady-state assumption for species H_2O_2, so truncation for H_2O_2 in reaction 27 of Table 3.1, which is $2HO_2 = H_2O_2 + O_2$, was made in the calculations. Therefore, a 7-step reduced mechanism for $CH_4/NO_2/O_2$ premixed flames can be represented by

$$
\begin{aligned}
I: &\quad CH_4 + 2OH \rightleftharpoons 2H_2 + H_2O + CO \\
II: &\quad H_2 + OH \rightleftharpoons H + H_2O \\
III: &\quad OH + CO \rightleftharpoons H + CO_2 \\
IV: &\quad H + H \rightleftharpoons H_2 \\
V: &\quad H_2 + O_2 \rightleftharpoons 2OH \\
VI: &\quad H + NO_2 \rightleftharpoons OH + NO \\
VII: &\quad 2NO \rightleftharpoons O_2 + N_2
\end{aligned}
$$

The reaction rates of the global reactions I - VII can be expressed in terms of elementary reaction rates in Table 3.1 as

$$
\begin{aligned}
w_I &= w_1 + w_2 + w_3 - w_4 \\
w_{II} &= w_2 + w_3 - w_6 - w_7 + w_9 - w_{10} - w_{12} - w_{13} - w_{17} + w_{18} + w_{19} \\
&\quad + w_{22} + w_{24} + w_{30} - w_{34} - w_{36} - w_{40} - w_{41} + w_{43} \\
w_{III} &= w_{16} + w_{44} + w_{45} \\
w_{IV} &= w_4 - w_{10} + w_{15} + w_{21} + w_{22} + w_{23} - w_{27} + w_{29} + w_{30} - w_{34} \\
&\quad - w_{35} - w_{36} \\
w_V &= w_6 + w_7 + w_{17} + w_{25} + w_{27} - w_{29} - w_{30} + w_{33} - w_{35} + w_{40} \\
&\quad + w_{41} - w_{43}
\end{aligned}
\tag{3.9}
$$

$$
\begin{aligned}
w_{VI} &= -w_{33} + w_{34} + 2w_{35} + w_{36} + w_{38} + w_{39} - w_{40} - w_{41} + w_{42} \\
&\quad + w_{43} + w_{44} + w_{45} \\
w_{VII} &= -w_{31} - w_{33} + w_{36} + w_{37} - w_{41} + w_{42}
\end{aligned}
$$

3.4.1 Comparisons between the Full Mechanism and the Reduced Mechanism

Calculations were done for flame systems with the first definition of equivalence ratio. The burning velocity as a function of equivalence ratio, ϕ, at pressure, $p = 1$ atm. is plotted in Fig. 3.20. The solid line represents the results from the full mechanism and the dotted line represents the results from the reduced mechanism. It can be seen that they agree with each other.

Structures of the premixed $CH_4/NO_2/O_2$ flames with equivalence ratio, $\phi = 1$, and pressure, $p = 1$atm. obtained from the reduced mechanism are shown as dotted lines in Figs. 3.21 - 3.25, the solid lines in these figures represent the structures of the same flame predicted by the full mechanism. The temperature profile obtained using the reduced mechanism agrees with that using the full mechanism. For stable species NO_2, CH_4, O_2, H_2O, NO, CO, CO_2, N_2, H_2, and the radicals OH, H, O, the results predicted by the reduced mechanism agree well with those from the full mechanism. Species profiles for CH_3O, CH_2O, and CH_3 are shown in Fig. 3.24. The peak values of these species from the reduced mechanism are roughly three times larger than those from the full mechanism. Species profiles for N, HCO, HO_2, and H_2O_2 are shown in Fig. 3.25. For nitrogen atom N, the mole fraction calculated from the full mechanism are always higher than that obtained from the reduced mechanism. The peak mole fractions of species HCO and HO_2 predicted by the reduced mechanism are higher than those by the full mechanism. For H_2O_2, the peak mole fraction obtained from the full mechanism is of two orders larger than that obtained from the reduced mechanism.

3.4.2 Variation of Burning Velocity as a Function of Pressure

Calculations were done to study flame structures with changes of pressure by using the reduced mechanism at equivalence ratio being unity. The burning velocities as a function of pressure is shown in Fig. 3.26. It can be seen that the burning velocity decreases with the increasing of pressure. Converged solutions were not obtained for values of pressure greater than 1.4 atm.

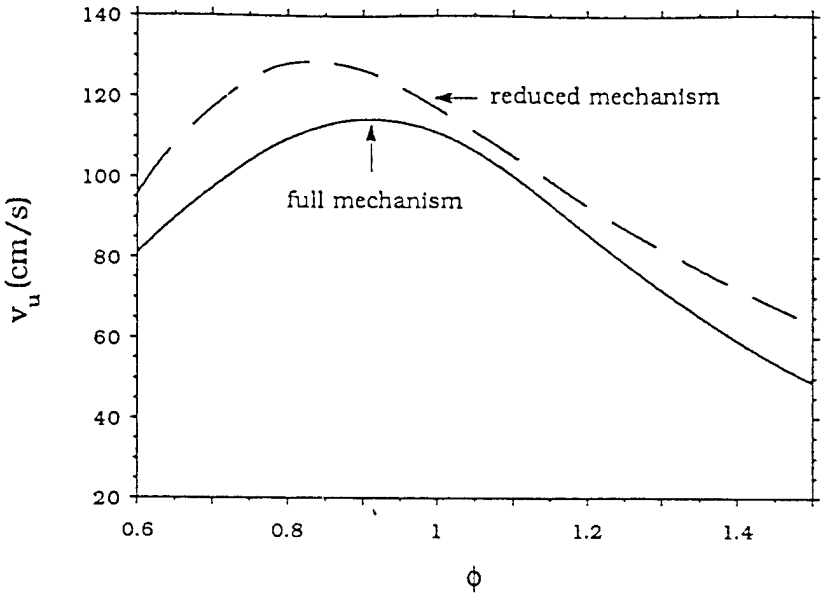

Figure 3.20: Variation of burning velocities of premixed $CH_4/NO_2/O_2$ flames calculated using the full mechanism and the reduced mechanism at $p = 1$ atm.

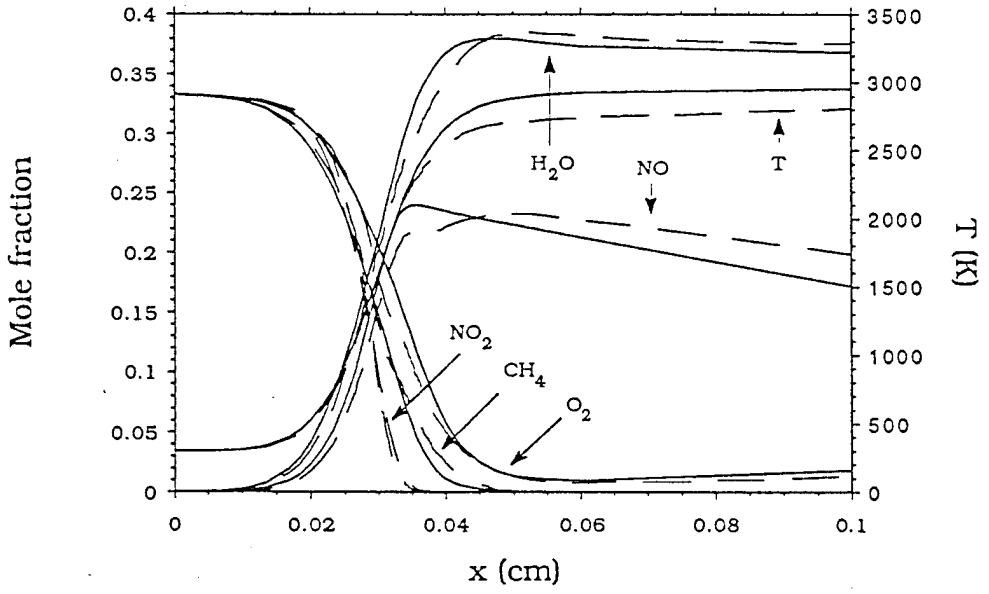

Figure 3.21: Profiles of T, H_2O, NO, NO_2, CH_4, and O_2 calculated using the full mechanism and the reduced mechanism at ϕ=1 and $p = 1$ atm.

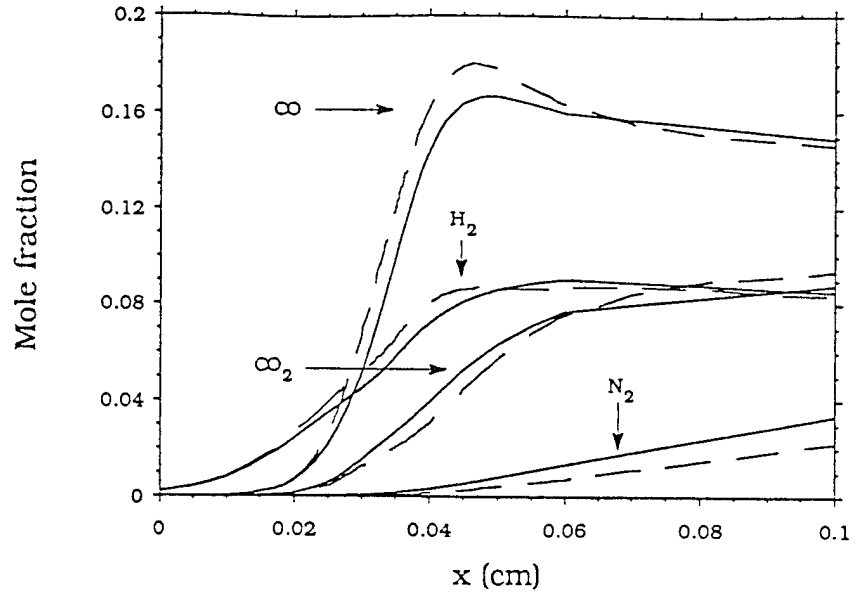

Figure 3.22: Profiles of CO, CO_2, H_2, and N_2 calculated using the full mechanism and the reduced mechanism at ϕ=1 and p = 1 atm.

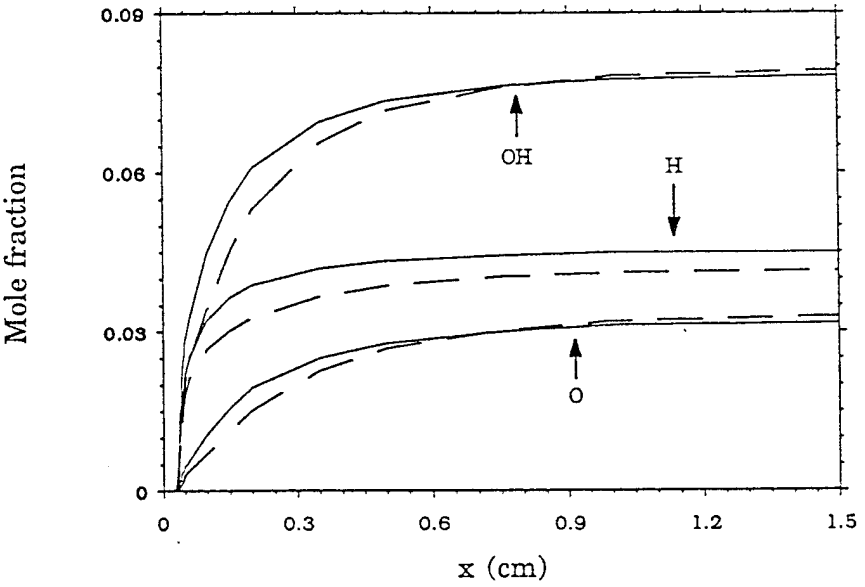

Figure 3.23: Profiles of OH, H, and O calculated using the full mechanism and the reduced mechanism at ϕ=1 and p = 1 atm.

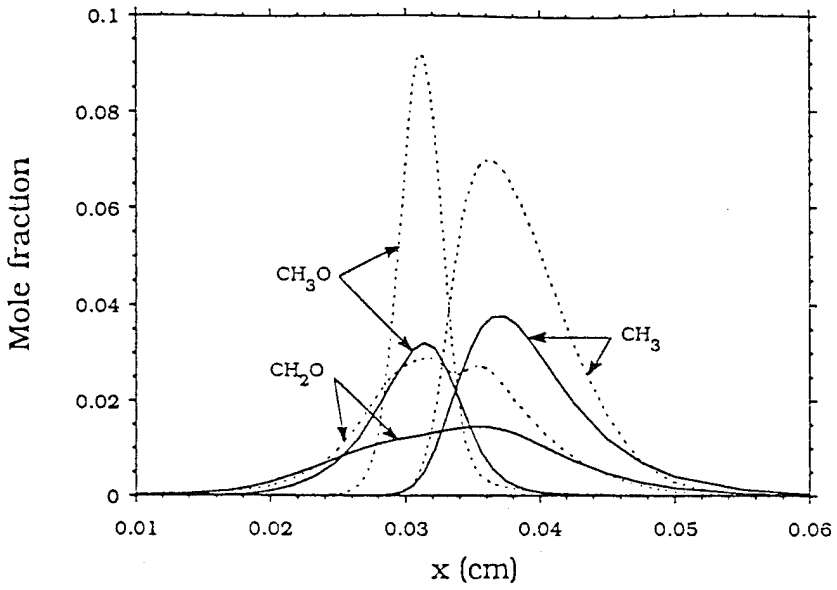

Figure 3.24: Profiles of CH_3O, CH_2O, and CH_3 calculated using the full mechanism and the reduced mechanism at ϕ=1 and p = 1 atm.

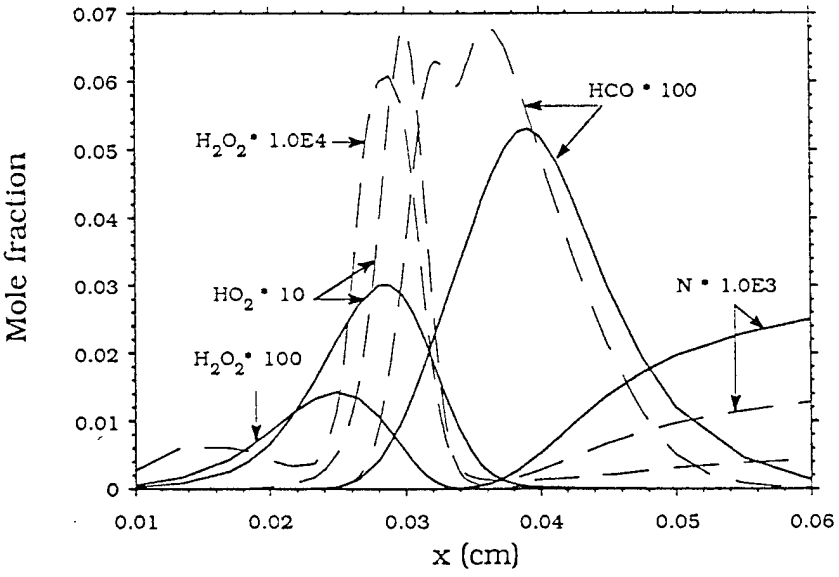

Figure 3.25: Profiles of HCO, H_2O_2, HO_2 and N calculated using the full mechanism and the reduced mechanism at ϕ=1 and p = 1 atm.

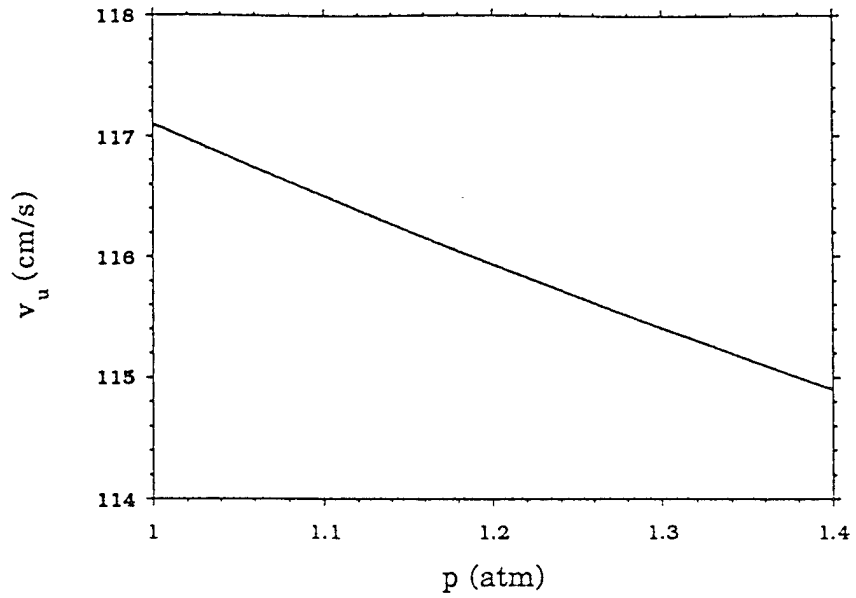

Figure 3.26: Variation of burning velocities of premixed $CH_4/NO_2/O_2$ flames as a function of pressure calculated using the full mechanism at $\phi = 1$

3.5 The Reduced Mechanism for Premixed $CH_2O/NO_2/O_2$ Flames

All the calculations in this section are done for flame systems with the first definition of equivalence ratio, ϕ, and at pressure, $p = 1.0$ atm. Two cases are considered. For the first case, the steady-state assumptions are made for four species H_2O_2, HCO, N and HO_2. For the second case, six species H_2O_2, HCO, N, HO_2, O, and OH are assumed in steady-state. The burning velocities as functions of equivalence ratio ϕ are plotted in Fig. 3.27. The results corresponding to the first case agree with those calculated using the full mechanism. However, the results corresponding to the second case deviate from those calculated using the full mechanism, especially in the vicinity of stoichiometry.

3.6 Conclusions

Numerical calculations were performed to study the flame structures of premixed $CH_4/NO_2/O_2$ and $CH_2O/NO_2/O_2$ flames. Two kinds of definition of equivalence ratio were defined to study the influences of equivalence ratio on burning velocities. The flame systems with the first kind definition behave like a usual two-reactant (fuel and oxidizer) flame systems. The structures of the flames were plotted to study the combustion processes in the flame. One outstanding feature of $CH_4/NO_2/O_2$ and $CH_2O/NO_2/O_2$ combustion systems is that NO_2 acts like a fuel,

and competes for radicals with fuel in the combustion processes and thus decreases the concentrations of the radicals, which makes the flames weaker. For a pure CH_4/NO_2 premixed flame, although numerically, it is possible to get a stable flame, this flame is very weak. For a pure CH_2O/NO_2 premixed flames, the burning velocity is very small compared with those near stoichiometric conditions, but it is still of the same order of the burning velocities of methane-air flame near stoichiometry. This explains the difficulties encountered in stabilizing pure CH_4/NO_2 premixed flames in the laboratory.

The structures of $CH_4/NO_2/O_2$ and $CH_2O/NO_2/O_2$ premixed flame systems resembles those of hydrocarbon flames. They include a preheat zone, an inner layer and a post-flame zone. The inner layer can further be subdivided into a fuel and oxidizer consumption layer in which the fuel and oxidizer are consumed to form CO, H_2, NO and some H_2O, an oxidation layer in which CO, H_2, and NO are oxidized to form CO_2, H_2O and N_2.

A seven-step reduced mechanism is developed for $CH_4/NO_2/O_2$ premixed flames. The burning velocities calculated using the reduced mechanism are in agreement with those calculated from the full mechanism. The temperature profile, the profiles for species H_2O, NO_2, CH_4, O_2, NO, CO, CO_2, H_2, N_2 and OH, H, O predicted by the reduced mechanism agree with those obtained using the full mechanism. For species H_2O_2, HCO, HO_2, N, CH_3, CH_2O, and CH_3, there are differences between the values obtained using the reduced mechanism and those from the full mechanism.

Two sets of reduced mechanisms for $CH_2O/NO_2/O_2$ premixed flames are tested. The first reduced mechanism is obtained by assuming four species HCO, H_2O_2, N and HO_2 in steady-state, the second reduced mechanism is obtained by assuming six species HCO, H_2O_2, N, HO_2, O and OH in steady-state. For the first reduced mechanism, the burning velocities predicted using the reduced mechanism agree well with those calculated from the full mechanism, and the temperature and species profiles for the stable species and radicals obtained both from the reduced and the full mechanism are in good agreement. For intermediate species HCO, HONO, HNO and HO_2, the results from the full mechanism and the reduced mechanism are also in agreement with each other. For species H_2O_2, the peak value obtained from the reduced mechanism is of two orders larger than that calculated from the full mechanism.

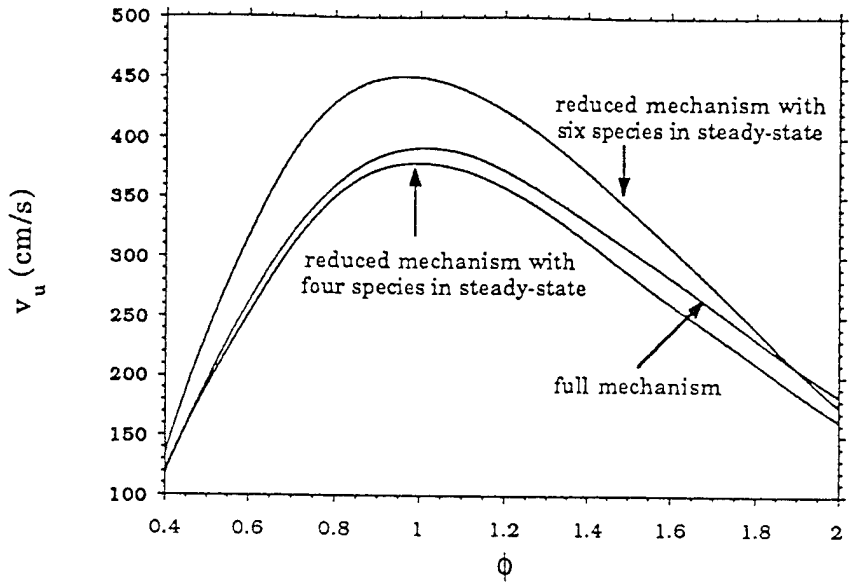

Figure 3.27: Burning velocities of premixed $CH_2O/NO_2/O_2$ flames calculated using the full and the reduced mechanisms at $p = 1$ atm.

Bibliography

Becker, D. L. (1988). Kinetic and related aspects of propellant combustion chemistry. *JANNAF Combustion Subcommittee Workshop, CPIA Publication 503.*

Branch, M. C., Sadeqi, M. E., Alfarayedhi, A. A. & Tiggelen, P. J. V. (1991). Measurements of the structure of laminar, premixed flames of $CH_4/NO_2/O_2$ and $CH_2O/NO_2/O_2$ mixtures. *Combustion and Flame* **83**, 228–239.

Bui-Pham, M. N. (1992). *Studies in Structures of Laminar Hydrocarbon Flames.* Ph.D thesis, University of California at San Diego, La Jolla, California.

Chelliah, H. K., Law, C. K., Ueda, T., Smooke, M. D. & Williams, F. A. (1990). An experimental and theoretical investigation of the dilution, pressure and flow-field effects on the extinction condition of methane-air-nitrogen diffusion flames. *Twenty-Third Symposium (International) on Combustion*, The Combustion Institute, Pittsburgh, PA, pp. 503–511.

Chelliah, H. K., Seshadri, K. & Law, C. K. (1993). Reduced kinetic mechanisms for counterflow methane-air diffusion flames. *in* N. Peters & B. Rogg (eds), *Reduced Kinetic Mechanisms for Applications in Combustion Systems*, Vol. **m 15** of *Lecture Notes in Physics*, Springer-Verlag Berlin Heidelberg, chapter 13, pp. 224–240.

Grudno, A. & Seshadri, K. (1995). Characteristic residence times of laminar nonpremixed flames at extinction. *Combustion Science and Technology, submitted* .

Ilincic, N. (1995). *Ignition and Extinction Phenomena in Combustion Systems.* Ph.D thesis, University of California at San Diego, La Jolla, California.

Kooker, D. E. (1995). Private communication.

Kooker, D. E., Chang, L. M. & Howard, S. L. (1993). Flamespreading in granular solid propellant. design of an experiment. *Technical Report ARL-TR-80*, Army Research Laboratory.

Kooker, D. E., Chang, L. M. & Howard, S. L. (1994). Flamespreading in granular solid propellant. initial results. *Technical Report ARL-TR-446*, Army Research Laboratory.

Kooker, D. E., Chang, L. M. & Howard, S. L. (1995). Flamespreading in granular solid propellant. Influence of propellant composition. *32nd JANNAF Combustion Subcommittee Meeting.*

Kubota, N. (1981). Combustion mechanisms of nitramine composite propellants. *Eighteenth Symposium (International) on Combustion*, The Combustion Institute, Pittsburgh, Pennsylvania, pp. 187–206.

Kuo, K. & Summerfield, M. (1984). *Progress in Astronautics and Aeronautics*, Vol. 90.

Melius, C. (1986). Thermochemistry of the decomposition of nitramines in the gas phase. *Twenty-First Symposium (International) on Combustion*, The Combustion Institute, Pittsburgh, Pennsylvania, pp. 1953–1963.

Melius, C. (1987). Theoretical studies involved in the ignition of nitramines. *24th JANNAF Combustion Meeting*, Monterey, California.

Melius, C. (1988). The gas-phase chemistry of nitramine combustion. *25th JANNAF Combustion Meeting*, Huntsville, Alabama.

Melius, C. (1989). Thermochemical modeling: Application to decomposition of energetic materials. Lecture presented at the NATO Advanced Study Institute on Chemistry and Physics of the Molecular Processes in Energetic Materials at Altavilla Milicia, Sicily.

Miller, J. A. & Bowman, C. T. (1989). Mechanism and modeling of nitrogen chemistry in combustion. *Progress in Energy and Combustion Science* **15**, 287–338.

Peters, N. (1991). Reducing mechanisms. *in* M. D. Smooke (ed.), *Reduced Kinetic Mechanisms and Asymptotic Approximations for Methane-Air Flames*, Vol. 384 of *Lecture Notes in Physics*, Springer-Verlag, Berlin Heidelberg, chapter 3, pp. 48–67.

Sadeqi, M. E. (1987). *Structure of multiple luminous zones of flames of methane and formaldehyde with nitrogen dioxide and oxygen.* Ph.D thesis, University of Colorado, Boulder, Colorado.

Sadeqi, M. E. & Branch, M. C. (1991). A continous flow gaseous formaldehyde generation system for combustion studies. *Combustion and Flame* **71**, 325–329.

Seshadri, K. & Göttgens, J. (1991). Structure of the oxidation layer for stoichiometric and lean methane-air flames. *in* M. D. Smooke (ed.), *Reduced Kinetic Mechanisms and Asymptotic Approximations for Methane-Air Flames*, Vol. 384 of *Lecture Notes in Physics*, Springer-Verlag, Berlin Heidelberg, chapter 6, pp. 111–136.

Seshadri, K. & Peters, N. (1988a). Asymptotic structure and extinction of methane-air diffusion flames. *Combustion and Flame* **73**, 23–44.

Seshadri, K. & Peters, N. (1988b). The inner structure of methane-air flames. *Combustion and Flame* **81**, 96–118.

Seshadri, K. & Williams, F. A. (1978). Laminar flow between parallel plates with injection of a reactant at high reynolds number. *International Journal of Heat and Mass Transfer* **21**(2), 251–253.

Seshadri, K. & Williams, F. A. (1994). Reduced chemical systems and their application in turbulent combustion. *in* P. A. Libby & F. A. Williams (eds), *Turbulent Reacting Flows*, Academic Press, San Diego, California, pp. 153–210.

Smooke, M. D. & Giovangigli, V. (1991a). Formulation of the premixed and nonpremixed test problems. *in* M. D. Smooke (ed.), *Reduced Kinetic Mechanisms and Asymptotic Approximations for Methane-Air Flames*, Vol. 384 of *Lecture Notes in Physics*, Springer Verlag Berlin Heidelberg, chapter 1, pp. 1–28.

Smooke, M. D. & Giovangigli, V. (1991b). Premixed and nonpremixed test problem results. *in* M. D. Smooke (ed.), *Reduced Kinetic Mechanisms and Asymptotic Approximations for Methane-Air Flames*, Vol. 384 of *Lecture Notes in Physics*, Springer Verlag Berlin Heidelberg, chapter 2, pp. 29–47.

Smooke, M. D., Puri, I. K. & Seshadri, K. (1986). A comparison between numerical calculations and experimental measurements of the structure of a counterflow diffusion flame burning diluted methane in diluted air. *Twenty-first Symposium (International) on Combustion*, The Combustion Institute, Pittsburgh, Pennsylvania, pp. 1783–1792.

Trees, D., Brown, T. M., Seshadri, K., Smooke, M. D., Balakrishnan, G., Pitz, R. W., Giovangigli, V. & Nandula, S. P. (1995). The structure of nonpremixed hydrogen-air flames. *Combustion Science and Technology* **104**(4-6), 427–439.

Treviño, C. & Williams, F. A. (1988). Asymptotic analysis of the structure and extinction of methane-air flames. *in* A. L. Kuhl, J. R. Bowen, J. L. Leyer & A. Borisov (eds), *Dynamics of Reactive Systems Part I: Flames*, Vol. 113 of *Progress in Astronautics and Aeronautics*, AIAA, Washington, DC, pp. 129–165.

Williams, F. A. (1985). *Combustion Theory.* 2 edn, Addison-Wesley Publishing Company, Redwood City, CA.

Yang, B. (1993). *The Structures of Methane, Methanol and Formaldehyde Flames.* Ph.d thesis, University of California at San Diego, La Jolla, California.

Zabarnick, S. (1991). Laser-Induced fluorescence diagnostics and chemical kinetic modeling of a $CH_4/NO_2/O_2$ flame at 55 torr. *Combustion and Flame* **85**, 27–50.